RUHR
UNIVERSITÄT
BOCHUM

RUB

Bachelorarbeit

Development of a Fundamental Equation of State for Propylene Glycol

Name: Tim Eisenbach
Matr.-Nr.: 108 014 219 607
Studiengang: Maschinenbau

1. Gutachter: Prof. Dr.-Ing. R. Span
2. Gutachter: Dr.-Ing. M. Thol

Betreuer: Dr. E. W. Lemmon
Dr.-Ing. M. Thol

August 2018

RUHR
UNIVERSITÄT
BOCHUM

RUB

Bachelor thesis

of Tim Eisenbach, Matr.-Nr.: 108 014 219 607

Development of a Fundamental Equation of State for Propylene Glycol

Knowledge of thermodynamic properties of fluids is an important basis for efficient and energetically optimal design of thermodynamic processes. Nowadays, this knowledge is available through fundamental equations of state. Glycols are commonly applied as working fluids in various refrigeration and ORC processes. Moreover, in the context of "Carbon Capture and Storage" (CCS), glycols play an important role as trace elements in carbon-rich mixtures. However, an accurate equation of state for propylene glycol is currently not available in the literature. The scope of this thesis is to develop a fundamental equation of state for propylene glycol. An accurate representation of properties of the pure substances is essential for modelling equations of state for mixtures over the entire fluid range; therefore, special focus has to be given to the correct representation of the physical behavior of this fluid as well as reasonable extrapolation behavior.

Scope of work

The scope of Mr. Eisenbach's work is to set up a new equation of state for propylene glycol using all experimental data available and modern fitting techniques. This will be accomplished through the following steps:

- Obtain a comprehensive understanding of the theoretical background of equations of state.
- Carry out a comprehensive literature research to find all experimental data currently published.
- Develop an equation of state for propylene glycol.
- Summarize the results in English.

Tools

The proposed project is a collaboration between Ruhr University Bochum and the National Institute of Standards and Technology (NIST). Dr. E. W. Lemmon from NIST and Dr.-Ing. M. Thol from RUB will be Mr. Eisenbach's supervisors. The non-linear fitting algorithm is provided by Dr. E. W. Lemmon from NIST.

Prof. Dr.-Ing. R. Span June 2018

Erklärung

Hiermit erkläre ich, *Tim Eisenbach*, die vorliegende Arbeit, abgesehen von den Beiträgen des ausgebenden Professors und der Betreuerin/des Betreuers, selbstständig angefertigt zu haben. Die Erstellung erfolgte ohne das unerlaubte Zutun Dritter. Alle Hilfsmittel, die für die Erstellung der vorliegenden Arbeit benutzt wurden, sind im Literaturverzeichnis dokumentiert. Alles, das aus anderen Arbeiten unverändert oder mit Abänderungen übernommen wurde, ist kenntlich gemacht.

Bochum, August 2018

_____

Tim Eisenbach

Table of Contents

List of Figures

List of Tables

Nomenclature

Latin Symbols

Symbol	Unit	Denotation
A	-	First thermal virial coefficient
a	$\mathrm{J \cdot mol^{-1}}$	Molar Helmholtz energy
	$\mathrm{J \cdot m^3 \cdot mol^{-2}}$	Parameter of the van der Waals equation
B	$\mathrm{m^3 \cdot mol^{-1}}$	Second thermal virial coefficient
b	$\mathrm{m^3 \cdot mol^{-1}}$	Parameter of the van der Waals equation
C	$\mathrm{m^6 \cdot mol^{-2}}$	Third thermal virial coefficient
c	$\mathrm{J \cdot mol^{-1} \cdot K^{-1}}$	Molar heat capacity
	-	Integration constant
D	$\mathrm{m^9 \cdot mol^{-3}}$	Fourth thermal virial coefficient
d	-	Density exponent
F	-	Deviation between a data point and the value calculated from the equation of state
g	$\mathrm{J \cdot mol^{-1}}$	Molar Gibbs energy
h	$\mathrm{J \cdot mol^{-1}}$	Molar enthalpy
I	-	Number of terms
i	-	Index
j	-	Index
k	$\mathrm{J \cdot K^{-1}}$	Boltzmann constant
	-	Index
M	$\mathrm{g \cdot mol^{-1}}$	Molar mass
m	-	Vibration mode parameter
N	-	Number of data points
n	-	Coefficient of the Helmholtz energy equation
	mol	Amount of substance
p	MPa	Pressure
	-	Density exponent in the exponential function
R	$\mathrm{J \cdot mol^{-1} \cdot K^{-1}}$	Universal gas constant
s	$\mathrm{J \cdot mol^{-1} \cdot K^{-1}}$	Molar entropy
T	K	Temperature
t	-	Temperature exponent
u	$\mathrm{J \cdot mol^{-1}}$	Molar internal energy
v	$\mathrm{m^3 \cdot mol^{-1}}$	Molar volume

Symbol	Unit	Denotation
W	-	Weight of data point during optimization
w	$\mathrm{m \cdot s^{-1}}$	Speed of sound
x	-	Value of any thermodynamic property
Z	-	Compressibility factor

Greek Symbols

Symbol	Unit	Denotation
α	-	Reduced Helmholtz energy
β	-	Gaussian bell-shaped parameter
Γ	-	Grüneisen coefficient
Π	-	Phase identification parameter
γ	-	Gaussian bell-shaped parameter
δ	-	Reduced density
ε	-	Gaussian bell-shaped parameter
η	-	Gaussian bell-shaped parameter
θ	K	Characteristic temperature of vibrational mode
ρ	$\mathrm{mol \cdot dm^{-3}}$	Molar density
τ	-	Reciprocal reduced temperature

Superscripts

Symbol	Denotation
o	Ideal gas contribution
r	Residual contribution
$'$	Saturated liquid
$''$	Saturated vapor
$*$	Reduced property
I	First integration
II	Second integration
l	Liquid
G	Glassy

Subscripts

Symbol	Denotation
0	Reference state
anc. eq.	Ancillary equations
B	Boiling point
c	Critical parameter
DATA	Experimental data point
EOS	Calculated from the equation of state
Exp	Exponential
G	Glassy
GBS	Gaussian bell-shaped
l	Liquid
liq	Liquid phase
max	Maximum
p	Constant pressure
PE	Planck-Einstein terms
Pol	Polynomial
r	Reducing parameter
res	Resiudual contribution
rot	Rotation
s	Constant entropy
simp	Simplified
tr	Triple point
trans	Translation
v	Constant volume
vap	Evaporation
vib	Vibration
x	Any thermodynamic property
δ	Derivation with respect to reduced density
τ	Derivation with respect to inverse reduced temperature

1 Introduction

In consideration of today's climate issues, optimization of facilities in the process engineering field and power generation becomes more important. In the course of this, well-established technologies and procedures need to be reviewed in terms of the involved components. An important part is the highly accurate investigation and understanding of the utilized fluids in process applications. Even though there is a vast quantity of fluids with a comprehensive data basis, some fluid states are not easily accessible with conventional measurements with a reasonable uncertainty range. To maintain the access to highly precise fluid properties over the entire fluid state, data can be calculated with equations of state. Thus, fluid states of high importance for process engineering, as well as for fundamental research, can often be fully determined with high reliability.

In this work a fundamental equation of state for propylene glycol was developed. Propylene glycol is an important fluid in cooling process applications, but yet still not sufficiently represented by the available data. For states in lower temperatures regions, a reliable and accurate equation of state for the pure compound is especially needed. Further, highly accurate calculations of properties are important for the development of mixture models, often involving water or carbon dioxide. Propylene glycol is known to improve carbon dioxide injectivity in carbon capture and storage (CCS) processes. For this purpose, in order to use propylene glycol in mixture models for combustion gases, a suitable equation of state for the pure compound is urgently needed. Prior to the development of the equation of state, a comprehensive literature research was carried out to obtain a reliable data base for the fitting process.

This work starts with a short presentation of the chemical properties of propylene glycol, followed by a brief historical review of equations of state and the explanation of the theoretical background of equations of state in terms of the Helmholtz energy. Chapter 4 covers an overview of the general fitting process and the applied algorithm of Lemmon (2018). Chapter 5 contains, aside from the investigation of the available data, the presentation of the equation of state as well as the comparison of data sets. After the discussion of the extrapolation behavior, the work is summarized by pointing out a few difficulties in the process of fitting the equation of state for propylene glycol and a short outlook for further investigations of the fluid is given.

2 Properties of Propylene Glycol

Propylene glycol, also known as 1,2-propanediol, is a synthetic produced organic compound and with its two hydroxyl-groups it can be assigned to the group of diols (glycols). The pure compound is a colorless, odorless, sweetish, viscous, and highly hygroscopic liquid, miscible with water, acetone, and chloroform. Propylene glycol, registered under the CAS-Number 57-55-6, has the chemical formula $C_3H_8O_2$. The structural formula is presented in Figure 2.1.

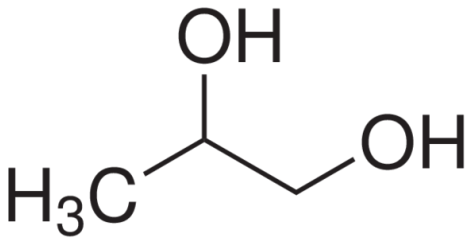

Figure 2.1 Structural formula of propylene glycol.

Propylene glycol is not acutely toxic for humans or animals due to its harmless metabolic by-products, mainly consisting of lactic or pyruvic acid according to Ruddick (1971). In contrast, ethylene glycol is metabolized to toxic acids according to the research of Cox (2004).

Each of the carbon-atoms forms a different functional group. The second carbon atom is seen as chiral or asymmetric because of its four different bonds, and determines the number of two stereoisomers of propylene glycol (Le Belvant Hoff rule). The first and third carbon atom, depending on the isomer, form methyl- and hydroxymethyl-groups. The two forms of stereoisomers of propylene glycol are the optically active forms R(-) and S(+). Specifically the two stereoisomers are enantiomers since they are related to each other by reflection. The structural isomer of 1,2-propanediol is 1,3-propanediol. The three dimensional structural formula of propylene glycol is shown in Figure 2.2.

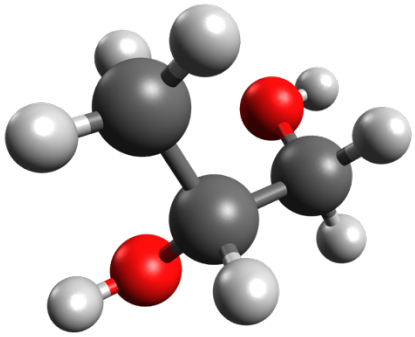

Figure 2.2 3D conformer of propylene glycol according to Avogadro by Hanwell *et al.* (2012).

Propylene glycol is most commonly manufactured from the noncatalytic hydrolysis of propylene oxide under high pressure up to 2.17 MPa and a relatively high temperature from 120 °C to 190 °C. A large excess amount of water is needed to convert propylene oxide into a mixture of 90% propylene glycol and 10% of di- and tri-propylene glycol. After removing water through a vaporization process, the glycols are purified by high vacuum distillation. In 1990, 342200 tons of propylene glycol were produced in the United States.

Accompanied by its non-toxic character, propylene glycol finds broad application in the food industry, pharmaceuticals, and cosmetics. The compound, labeled as humectant food additive E1520, is used as a solvent for food colors and flavorings, as well as a desiccant. Propylene glycol is also used as a solvent and coupling agent in sanitizers, lotions, pharmaceutical preparations, or other aqueous solutions according to Martin and Murphy (2000). The aqueous solution of propylene glycol is known for its excellent antifreeze properties and, thus, can be applied in cooling processes as a low temperature heat transfer fluid or in aircraft deicing procedures.

Propylene glycol molecules presumably have strongly associative interactions due to their two hydroxyl groups. Association is the aggregation of atoms and molecules into larger units due to weak hydrogen bonds or bridges between hydroxyl groups. In an associating fluid, the associated complexes and simple molecules come to an equilibrium. Since propylene glycol is highly hygroscopic, it is often found in an aqueous solution in which it shows a more clear affinity to be hydrated than to be self-associated. Nevertheless, a peak of hydroxyl group interaction between two propylene glycol molecules in a 30 mol-% aqueous solution can be found at intermolecular or group distances of around 1.95 Å according to Rhys *et al.* (2016). Taking this into account, pure propylene glycol, without any distribution of hydration, is likely to have

a relatively strong associative character. Due to its hygroscopic character, propylene glycol and glycols in general are used in the natural gas industry in water removing processes.

The common use of propylene glycol as an antifreeze is based on the cryoprotective properties of the pure compound as well as the aqueous solution. Neat propylene glycol is a glass former, absent of any crystal-like structure with more than 68 wt-% in an aqueous solution according to the research of Boutron and Kaufmann (1979). As a consequence of the two equimolarly present enantiomers, nuclei formation and crystal growth is prevented. The aqueous solution of propylene glycol remains amorphous with 50 wt-% or less water at all cooling rates. The glass transition behavior and, by implication, also the glass transition temperature T_G, are dependent on cooling or warming rates, how the glassy state was formed, and the content of water. For an aqueous solution of propylene glycol, the glass transition temperature is −105.5 °C with a cooling rate of 2.5 K per minute and a propylene glycol content of 45 wt-% according to Boutron and Kaufmann (1979).

The glass transition can also be seen as the freezing of relaxation processes within the molecule or between structural complexes. The relaxation of propylene glycol is determined by three distinctly different relaxation processes according to the research of Andersson and Andersson (1998). The structural α-relaxation describes segmental motions within the polymer chains or, in the case of propylene glycol, within the associated cluster. The freezing of this relaxation process is mostly responsible for the glass transition. Motions of the whole associated complexes are attributed to the α'-relaxation. Andersson and Andersson (1998) found out that both of these relaxations depend on the molar mass. The third observed relaxation is the fast β-relaxation at high frequencies, which is ascribed to the motion of a particle in the transient cage formed by neighboring molecules according to Köhler *et al.* (2008). To determine the glass transition temperature, the temperature where the abrupt heat capacity change occurs must be examined. The jump in heat capacity at T_G for propylene glycol can be estimated as $c_p^l / c_p^G = 1.85$ (Angell (1995)). Generally, the jump in heat capacity is a result of the change of the liquid's elastic, vibrational, and thermal properties according to Trachenko and Brazhkin (2011). Following the Adam-Gibbs theory, the abrupt change of heat capacity is due to the configurational entropy, which goes to zero at a temperature lower than T_G. Another explanation for the jump in heat capacity is its coherence to the difference in sampling the minima of the potential energy landscape (PEL). As the temperature decreases, "the system becomes trapped in one of the minima of the PEL, corresponding to the glassy state" (Debenedetti and

Stillinger (2001)). The theory by Trachenko and Brazhkin (2011) supports a purely dynamic approach: the jump in heat capacity is caused by the freezing of local relaxation events (LRE), which are closely related to the coefficient of thermal expansion ($\alpha_{G/l}$). Since the thermal expansion coefficient is strongly temperature dependent; the heat capacity and its behavior at T_G follow the abrupt change of α_l to α_G due to the freezing of the LRE. The local relaxation event can be viewed as the jump of atoms from their surrounding cage resulting in large-scale rearrangements in a liquid phase. Although glass transition temperatures can be determined from the jump in heat capacity, the attempts to explain the process of glass transition differ somewhat from each other.

The relevant characteristic thermodynamic properties of propylene glycol as well as the universal gas constant are listed in Table 2.1.

Table 2.1 Characteristic thermodynamic properties of propylene glycol and the universal gas constant.

Physical Properties	Denotation	Value	Unit	Reference
Critical temperature	T_c	676.4	K	VonNiederhausern *et al.* (2000)
Critical density	ρ_c	4.5	mol·dm^{-3}	This work
Critical pressure	p_c	7.82	MPa	This work
Normal boiling point	T_B	460.72	K	This work
Triple point temperature	T_{tr}	214	K	Martinez (1995)
Triple point density	$\rho_{tr,liq}$	14.372	mol·dm^{-3}	This work
Glass transition temperature	T_G	167.65	K	Boutron and Kaufmann (1979)
Molar mass	M	76.0944	g·mol^{-1}	Wieser and Berglund (2009)
Universal gas constant	R	8.3144598	J·mol^{-1}·K^{-1}	Mohr *et al.* (2012)

All temperature data are given on the ITS-90 scale.

3 Equations of State

This chapter summarizes the historical development of equations of state. Furthermore, the equation of state in terms of the Helmholtz energy, being the most common way to calculate thermodynamic properties of fluids, is introduced.

3.1 Common Types of Equations of State

The first equation of state was formulated by Clapeyron (1834) for a hypothetical ideal gas and is written in terms of the pressure p, the specific volume v, the universal gas constant R, and the temperature T:

$$pv = RT. \tag{3.1}$$

Each of the thermodynamic properties p, v, and T of an ideal gas can be calculated in terms of the other two. For a homogeneous pure compound, equations of state can be written in their implicit form

$$f(p, v, T) = 0. \tag{3.2}$$

In 1873, van der Waals developed a cubic equation of state, first taking interaction forces of molecules into account and, thus, approaching real gas behavior of fluids. Furthermore, the van der Waals cubic equation

$$p = \frac{RT}{v - b} - \frac{a}{v^2}, \tag{3.3}$$

was the first published equation of state, and could be applied to calculate the thermodynamic properties of supercritical states as well as vapor-liquid equilibrium. The parameters a and b in Eq. (3.3) are called van der Waals constants. The coherence pressure a is a reducing parameter to the ideal pressure of a gas, considering attractive forces between molecules, whereas the covolume b limits the total volume occupied by the gas to a volume that allows for the actual movement of the molecules. Due to the cubic character of isotherms in the vapor-liquid equilibrium region of a substance, the van der Waals equation has three specific volume roots. The highest and lowest root can be assigned to the volume of the liquid and vapor phase, while the middle root represents an unstable and physically unaccessible solution. As the fluid approaches the critical point, the densities of the vapor and liquid phases approach the same value. The

critical isotherm exhibits a saddle point and gives the second condition for solving the root of the specific volume and the two van der Waals constants:

$$a = \frac{27}{64}\frac{R^2 {T_\mathrm{c}}^2}{p_\mathrm{c}}$$

and (3.4)

$$b = \frac{1}{8}\frac{RT_\mathrm{c}}{p_\mathrm{c}}.$$

Depending on the substance, the van der Waals constants can, thus, be determined from the critical parameters. Today, common cubic equations similar to the van der Waals equation of state (e.g., Soave (1980) modification of Redlich-Kwong, Peng and Robinson (1976), etc.) are frequently used due to obtain computational efficiency, but often lack the required accuracy.

In 1901, Kamerlingh Onnes (1901) introduced the virial equation of state

$$\frac{p(T,\rho)}{\rho RT} = Z(T,\rho) = A + B(T)\rho + C(T)\rho^2 + D(T)\rho^3 + \cdots, \tag{3.5}$$

which describes the intermolecular forces with a series of viral coefficients. Z is the compressibility factor and *B*, *C*, and *D* are the second, third, and fourth virial coefficients describing the interactions of two, three, and four molecules, respectively. At the point where a gas approaches ideal behavior, the density approaches zero. The volume occupied by the substances becomes very large compared to the volumes of the molecules, indicating that there is no interaction between molecules. Applying the limit for an ideal gas ($\rho \to 0$) to the virial equation of state,

$$\lim_{\rho\to 0}\frac{p(T,\rho)}{\rho RT} = \lim_{\rho\to 0} Z(T,\rho) = 1, \tag{3.6}$$

the first virial coefficient can be set to $A = 1$, describing the ideal gas behavior for Z. The real gas character, taking intermolecular forces into account, is displayed by the higher virial coefficients. The great advantage of the cubic equations of state was the capability to model the gaseous and gas-like supercritical states with significantly higher accuracy. To cover the entire fluid region without an excessive number of virial coefficients, which could lead to disproportional physical behavior due to the high flexibility, a comprehensive extension of the virial equation of state Eq. (3.5) was needed. An extension of this type was first considered by Benedict *et al.* (1940) (BWR equation):

$$\frac{p(T,\rho)}{\rho RT} = Z(T,\rho) = 1 + \sum_{i=1}^{6} n_i T^{t_i} \rho^{d_i} + \sum_{i=7}^{8} n_i T^{t_i} \rho^{d_i} \exp\left[-\left({}^{\rho}/_{\rho_\mathrm{r}}\right)^2\right]. \tag{3.7}$$

The adjustable coefficients n_i are used to fit the equation of state to the specific substance and contribute to a qualitatively correct representation of properties in the entire fluid region according to Span (2000). The exponential terms were introduced to reduce the number of terms to eight. By introducing the reducing parameter for the density ρ_r, a fluid specific property contributes to the equation of state, since ρ_r is equal to the critical density of the substance.

Over the next 30 years, equations of state were developed that were derived from the BWR type-equation of state to describe properties of selected fluids even more accurately, especially for vapor-liquid equilibrium. An important requirement for the successful development of highly accurate equations of state was the continuous improvement of optimization algorithms according to Span (2000). One of the outstanding advances when developing an equation of state was the capability of fitting coefficients to $p\rho T$ and phase equilibrium data simultaneously. The two most representative equations of state of this period are the Bender-type equation of state of Bender (1970), which contains 19 substance dependent coefficients, and the modified BWR-type equation of state by Jacobsen and Stewart (1973).

In the 1980s, equations of state in terms of the Helmholtz energy became common due to the fact that pressure explicit equations of state need to be integrated to calculate caloric properties. The integration of each term of the pressure explicit equations of state is computationally expensive when it is done numerically. Aside from calculational speed, equations of state in terms of pressure (or compressibility factor) have no general disadvantage, since terms are always formulated in a way that numerical integration is possible according to Span (2000). Therefore, pressure explicit equations of state are still in use today to calculate thermodynamic properties, both thermal and caloric, of substances in engineering applications without requirements on high accuracy. For applications that require high accuracy, equations of state in terms of the Helmholtz energy are well established to calculate thermal and caloric properties for pure fluids as well as for mixtures.

3.2 Fundamental Equations of State in Terms of the Helmholtz Energy

The Helmholtz energy $a(T, v)$, the Gibbs energy $g(T, p)$, the internal energy $u(v, s)$, and the enthalpy $h(p, s)$ are the four well-known fundamental equations of state. All thermodynamic properties can be calculated from a combination of the equation and its derivatives with respect to the independent variables temperature T and density ρ. Due to the fact that the entropy s is a non-measurable independent variable, the internal energy as well as the enthalpy are less suitable as fundamental equations of state. The Gibbs energy is an important property when studying phase transitions. However, the first derivative is not continuous when crossing the phase boundary and, therefore, a supplementary equation is needed to obtain properties over the entire range of thermodynamic states. Since the fundamental equation of state in terms of the Helmholtz energy as a function of temperature and density is a continuous function over the entire fluid state, it is the most convenient method for calculating thermodynamic properties, including two-phase states and properties in the critical region.

The molar Helmholtz energy a is defined by

$$a(T, \rho) = u - Ts. \tag{3.8}$$

Helmholtz equations are often formulated and applied in their reduced form, $\alpha(\tau, \delta)$, as

$$\alpha(\tau, \delta) = \frac{a(T, \rho)}{RT} \tag{3.9}$$

with $\tau = T_\mathrm{r}/T$ and $\delta = \rho/\rho_\mathrm{r}$. In most cases the critical parameters T_c and ρ_c are used for T_r and ρ_r in order to reduce the density and temperature. The molar Helmholtz energy itself is reduced by temperature and the gas constant R and is further separated into two parts

$$\alpha(\tau, \delta) = \alpha^\circ(\tau, \delta) + \alpha^\mathrm{r}(\tau, \delta). \tag{3.10}$$

The ideal part α° describes the hypothetical ideal gas behavior at a given state determined by temperature and density. The residual part α^r describes the interactions of molecules that contribute to the behavior of the real fluid.

3.2.1 Ideal Part

Similar to Eq. (3.8), the molar Helmholtz energy for the ideal gas can be written as

$$a^\circ(T,\rho) = u^\circ(T) + Ts^\circ(T,\rho). \tag{3.11}$$

The internal energy of the ideal gas $u^\circ(T)$ is defined by

$$u^\circ(T) = u_0^\circ + \int_{T_0}^{T} c_v^\circ \,\mathrm{d}T, \tag{3.12}$$

where u_0° is the reference internal energy and c_v° is the isochoric heat capacity of the ideal gas. The ideal entropy in Eq. (3.11) can be formulated as

$$s^\circ(T,\rho) = s_0^\circ + \int_{T_0}^{T} \frac{c_v^\circ}{T}\mathrm{d}T - R\ln\left(\frac{\rho}{\rho_0}\right) \tag{3.13}$$

and the reference density ρ_0 can be calculated from the thermal equation of state for the ideal gas:

$$\rho_0 = \frac{p_0}{RT_0}. \tag{3.14}$$

With equations (3.12) to (3.14), the Helmholtz energy for the ideal gas can be expressed as

$$a^\circ(T,\rho) = u_0^\circ - Ts_0^\circ + \int_{T_0}^{T} c_v^\circ \mathrm{d}T - T\int_{T_0}^{T} \frac{c_v^\circ}{T}\,\mathrm{d}T + R\ln\left(\frac{\rho}{\rho_0}\right). \tag{3.15}$$

In order to obtain the temperature dependence of the ideal part, an equation for the isochoric heat capacity of the ideal gas needs to be developed. An empirical formulation of the ideal isobaric heat capacity is given by Wagner and Span (1993). It can be transferred into the isochoric heat capacity of the ideal gas according to $c_v^\circ = c_p^\circ - R$:

$$\frac{c_p^\circ(T)}{R} = n_0^* + \sum_{i=1}^{I_{\mathrm{Pol}}} n_i^* T^{t_i^*} + \sum_{i=I_{\mathrm{Pol}}+1}^{I_{\mathrm{Pol}}+I_{\mathrm{PE}}} m_i \left(\frac{\theta_i}{T}\right)^2 \frac{\exp(\theta_i/T)}{[\exp(\theta_i/T)-1]^2}. \tag{3.16}$$

Each of the terms in Eq. (3.16) contributes to the internal energy on the macroscopic scale or the kinetic energy on the microscopic scale of the ideal gas. The polynomial terms in Eq. (3.16) represent the temperature dependence of the isobaric heat capacity at moderate to low temperatures, and can be used for sufficiently high accuracy over a limited temperature range. To

avoid an increasing number of polynomial terms to represent higher temperatures, it is more convenient to introduce the Planck-Einstein terms to Eq. (3.16). With these terms, the heat capacity can be calculated in a broad temperature range with high accuracy and good extrapolation behavior. Nowadays, polynomial terms are avoided in modern equations of state.

In the following, considering classical mechanics, the contributions of translation, external rotation, and vibrational modes to the dynamic state of an ideal gas are explained. The dynamic state can be seen as internal energy on a macroscopic scale and is responsible for the ideal-gas heat capacity according to Span (2000). Defining a simplified isobaric heat capacity for the ideal gas

$$c_{p,\mathrm{simp}}^{\circ} = c_{v,\mathrm{simp}}^{\circ} + R = c_{\mathrm{trans}} + c_{\mathrm{rot}} + c_{\mathrm{vib}} + R \tag{3.17}$$

implies the assumption that the contributing effects do not interact with each other. While the contribution of translation and internal rotation can be derived straightforwardly from the transitional and rotational degrees of freedom of the molecule, the internal vibrations are described by the Planck-Einstein terms. Nonetheless, a few assumptions are made to determine c_{trans} and c_{rot}. For the ideal gas, all three degrees of freedom for translational movements are fully excited due to the fact that intermolecular forces are neglected. This assumption is for most fluids valid at temperatures $T > 10^{-10}$ K according to Span (2000). Each degree of freedom contributes $1/2\,R$ to the heat capacity, yielding

$$c_{\mathrm{trans}} = \frac{3}{2} R. \tag{3.18}$$

Assuming a rigid molecule without changes in shape due to increasing rotational speed or vibration, the moment of inertia can be treated as temperature independent and, thus, each fully excited mode of external rotation contributes $1/2\,R$ to heat capacity. Non-linear molecules are excitable in three rotational directions, however linear molecules only rotate around two axes. For a non-linear molecule, such as propylene glycol, the contribution of external rotation to the ideal-gas heat capacity is

$$c_{\mathrm{rot}} = \frac{3}{2} R. \tag{3.18}$$

Assuming only harmonic oscillation behavior of molecules, the influence of internal vibration on the heat capacity is considered by the Planck-Einstein terms:

$$\frac{c_i}{R} = \left(\frac{\theta_i}{T}\right)^2 \frac{\exp(\theta_i/T)}{[\exp(\theta_i/T) - 1]^2}. \tag{3.19}$$

In accordance to Span (2000), the assumption of harmonic oscillation yields convenient results in a moderate temperature range. With the assumption of a rigid rotator and harmonic oscillator, the simplified heat capacity of the ideal gas in Eq. (3.17) yields

$$\frac{c_{p,\mathrm{simp}}^\circ}{R} = \left(1 + \frac{c_{\mathrm{trans}}}{R} + \frac{c_{\mathrm{rot}}}{R}\right) + \sum_{i=1}^{I_{\mathrm{PE}}} m_i \left(\frac{\theta_i}{T}\right)^2 \frac{\exp(\theta_i/T)}{[\exp(\theta_i/T) - 1]^2}. \tag{3.21}$$

In theory, the parameter m_i equals one, except for multiple vibration modes with identical wave numbers. In reality, the characteristic temperature of the i-th vibrational mode θ_i, and the parameter m_i, are adjustable values. This approach primarily shortens the equation and accounts for empirical corrections of the prementioned simplifications as well. For propylene glycol, Eq. (3.21) results in

$$\frac{c_{p,\mathrm{simp}}^\circ}{R} = 4 + \sum_{i=1}^{I_{\mathrm{PE}}} m_i \left(\frac{\theta_i}{T}\right)^2 \frac{\exp(\theta_i/T)}{[\exp(\theta_i/T) - 1]^2}. \tag{3.22}$$

With the intention to model heat capacity for a simple molecule at moderate temperatures, the approach in Eq. (3.22) yields accurate and convenient results. For higher temperatures and more complex molecules, the model of a rigid, harmonic oscillator can not be applied and further considerations are needed (Span (2000)).

To obtain the reduced Helmholtz energy equation of state, it is easier to formulate Eq. (3.16) in terms of the isochoric heat capacity of the ideal gas c_v° as a function of the reduced temperature:

$$\frac{c_v^\circ(\tau)}{R} = n_0 + \sum_{i=1}^{I_{\mathrm{Pol}}} n_i \tau^{t_i} + \sum_{i=I_{\mathrm{Pol}}+1}^{I_{\mathrm{Pol}}+I_{\mathrm{PE}}} m_i \left(\frac{\theta_i \tau}{T_\mathrm{c}}\right)^2 \frac{\exp(\theta_i \tau/T_\mathrm{c})}{[\exp(\theta_i \tau/T_\mathrm{c}) - 1]^2}. \tag{3.23}$$

The reduced parameters can be defined by $n_0 = {n_0}^* - 1$, $n_i = {n_i}^* {T_\mathrm{c}}^{{t_i}^*}$, and $t_i = -{t_i}^*$ and τ is the inverse reduced temperature T_c/T. The isochoric heat capacity of the ideal gas is directly related to the second derivative of the reduced Helmholtz energy with respect to the reduced temperature τ according to Span 2000:

$$\left(\frac{\partial^2 \alpha^\circ}{\partial \tau^2}\right)_\delta = -\frac{c_v^\circ}{R\tau^2}. \tag{3.24}$$

Twofold integration of Eq. (3.24) yields the Helmholtz energy of the ideal gas:

$$a^{\circ}(\tau,\delta) = c^{\mathrm{II}} + c^{\mathrm{I}}\tau + n_0 \ln(\tau) + \ln(\delta) - \sum_{i=1}^{I_{\mathrm{Pol}}} \frac{n_i}{t_i(t_i-1)}\tau^{t_i} + \sum_{i=I_{\mathrm{Pol}}+1}^{I_{\mathrm{Pol}}+I_{\mathrm{PE}}} m_i \ln[1-\exp(-\theta_i\tau)]. \tag{3.25}$$

The integration constants c^{I} and c^{II} describe the relation of zero states of caloric properties to the Helmholtz energy or to its first derivative with respect to τ (Span (2000)). The reference state can arbitrarily be chosen. For propylene glycol the normal boiling point is considered as an appropriate reference point. At $\rho'(p = 1\ \mathrm{atm})$ and $T_{\mathrm{sat}}(p = 1\ \mathrm{atm})$ the enthalpy and entropy are equal to zero.

3.2.2 Residual Part

The residual part of the Helmholtz energy describes real fluid behavior differing from the ideal part, which is derived from statistical thermodynamics. Although thermodynamic properties are related to terms in the residual part, its parameters are treated empirically. Generally, the residual part can be defined by

$$\alpha^{\mathrm{r}}(\tau,\delta) = \alpha^{\mathrm{r}}_{\mathrm{Pol}}(\tau,\delta) + \alpha^{\mathrm{r}}_{\mathrm{Exp}}(\tau,\delta) + \alpha^{\mathrm{r}}_{\mathrm{GBS}}(\tau,\delta) + \alpha^{\mathrm{r}}_{\mathrm{NA}}(\tau,\delta)$$

$$= \sum_{i=1}^{I_{\mathrm{Pol}}} n_i \tau^{t_i}\delta^{d_i} + \sum_{i=I_{\mathrm{Pol}}+1}^{I_{\mathrm{Pol}}+I_{\mathrm{Exp}}} n_i\,\tau^{t_i}\delta^{d_i}\exp(-\gamma_i\delta^{p_i}) + \sum_{i=I_{\mathrm{Pol}}+I_{\mathrm{Exp}}+1}^{I_{\mathrm{Pol}}+I_{\mathrm{Exp}}+I_{\mathrm{GBS}}} n_i\,\tau^{t_i}\delta^{d_i}\exp(-\eta_i(\delta-\varepsilon_i)^2 - \beta_i(\tau-\gamma_i)^2). \tag{3.26}$$

The polynomial and exponential terms of the reduced Helmholtz energy equation (3.26) are similar to the pressure explicit equation of state Eq. (3.7) of Benedict *et al.* (1940), accurately representing the homogeneous region as well as the vapor-liquid phase equilibrium of the real fluid. The density exponents d_i and p_i need to be positive integers for the residual part of an ideal Helmholtz energy equation near zero density go to zero along with all its derivatives with respect to density. The temperature exponents t_i must be positive and have an infinite contribution to the Helmholtz energy near zero kelvin. The broad range for temperature and density exponents allows high flexibility to the equation of state, with some restrictions, explained more

closely in chapter 4. As already mentioned in Section 3.1, derivatives can be calculated analytically for any combination of parameters.

The polynomial and exponential terms can describe the fluid behavior for most states. Nonetheless, those terms fail near the critical region in regards to the required accuracy. Thus, additional terms are needed to both yield larger gradients of derivations of Helmholtz energy and leave the non-critical region unaffected. Therefore, the Gausssian bell shaped (GBS) terms were first introduced by Haar *et al.* (1982) and later adjusted by Setzmann and Wagner (1991) with remarkable accuracy in representing thermal and caloric properties in the critical region. The number of Gaussian bell shaped terms are usually kept in the range of three to five.

Besides the GBS terms, there are non-analytical terms $\alpha_{\mathrm{NA}}^{\mathrm{r}}$, which can describe the properties of the isochoric heat capacity and the speed of sound at their critical maximum and minimum, respectively, and were first introduced by Span (2000). Non-analytical terms were only used for the equations of carbon dioxide and water and are unlikely to be used again, since high numerical expansions occur for its derivatives and the advantages in accurately describing the properties are limited to a narrow region around the critical point.

3.2.3 Thermodynamic Properties and Their Relation to the Reduced Helmholtz Energy

As already pointed out, the great advantage of a fundamental equation of state in terms of the Helmholtz energy is the unrestricted ability to write each thermodynamic property, both thermal and caloric, in terms of the ideal or the residual part and their derivatives. Table 3.1 displays the relation between selected thermodynamic properties and the reduced Helmholtz energy. The abbreviations for the partial derivatives of the reduced Helmholtz energy mentioned in Table 3.1 are given in Eqs. (3.27) to (3.31). The following expressions are valid for both the ideal and residual reduced Helmholtz energy.

$$\alpha_\tau = \left(\frac{\partial \alpha}{\partial \tau}\right)_\delta \qquad (3.27), \qquad \alpha_{\tau\tau} = \left(\frac{\partial^2 \alpha}{\partial \tau^2}\right)_\delta \qquad (3.28), \qquad \alpha_{\delta\tau} = \left(\frac{\partial^2 \alpha}{\partial \delta \partial \tau}\right) \qquad (3.29),$$

$$\alpha_\delta = \left(\frac{\partial \alpha}{\partial \delta}\right)_\tau \qquad (3.30), \qquad \alpha_{\delta\delta} = \left(\frac{\partial^2 \alpha}{\partial \delta^2}\right)_\tau \qquad (3.31).$$

Table 3.1 Definition of thermodynamic properties and their relation to the reduced Helmholtz energy.

Property		**Relation to the reduced Helmholtz energy**	
Pressure			
$p(T,\rho) = -\left(\frac{\partial a}{\partial v}\right)_T$	(3.32)	$\frac{p}{\rho RT} = 1 + \delta\alpha_\delta^{\mathrm{r}}$	(3.33)
Entropy			
$s(T,\rho) = -\left(\frac{\partial a}{\partial T}\right)_v$	(3.34)	$\frac{s}{R} = \tau(\alpha_\tau^\circ + \alpha_\tau^{\mathrm{r}}) - \alpha^\circ - \alpha^{\mathrm{r}}$	(3.35)
Internal energy			
$u(T,\rho) = a - Ts$	(3.36)	$\frac{u}{RT} = \tau(\alpha_\tau^\circ + \alpha_\tau^{\mathrm{r}})$	(3.37)
Enthalpy			
$h(T,\rho) = u + pv$	(3.38)	$\frac{h}{RT} = 1 + \tau(\alpha_\tau^\circ + \alpha_\tau^{\mathrm{r}}) + \delta\alpha_\delta^{\mathrm{r}}$	(3.39)
Isobaric heat capacity			
$c_p(T,\rho) = -\left(\frac{\partial h}{\partial T}\right)_p$	(3.40)	$\frac{c_p}{R} = -\tau^2(\alpha_{\tau\tau}^\circ + \alpha_{\tau\tau}^{\mathrm{r}}) + \frac{(1 + \delta\alpha_\delta^{\mathrm{r}} - \delta\tau\alpha_{\delta\tau}^{\mathrm{r}})^2}{1 + 2\delta\alpha_\delta^{\mathrm{r}} + \delta^2\alpha_{\delta\delta}^{\mathrm{r}}}$	(3.41)
Gibbs energy			
$g(T,\rho) = h - Ts$	(3.42)	$\frac{g}{RT} = 1 + \alpha^\circ + \alpha^{\mathrm{r}} + \delta\alpha_\delta^{\mathrm{r}}$	(3.43)
Speed of sound			
$w(p,T) = \sqrt{\left(\frac{\partial p}{\partial \rho}\right)_s}$	(3.44)	$\frac{w^2}{RT} = 1 + 2\delta\alpha_\delta^{\mathrm{r}} + \delta^2\alpha_{\delta\delta}^{\mathrm{r}} - \frac{(1 + \delta\alpha_\delta^{\mathrm{r}} - \delta\tau\alpha_{\delta\tau}^{\mathrm{r}})}{\tau^2(\alpha_{\tau\tau}^\circ + \alpha_{\tau\tau}^{\mathrm{r}})}$	(3.45)
Second thermal virial coefficient			
$B(T) = \lim_{\rho\to 0}\left(\frac{\partial\left(\frac{p}{\rho RT}\right)}{\partial\rho}\right)_T$	(3.46)	$B\rho_{\mathrm{r}} = \lim_{\delta\to 0}\alpha_\delta^{\mathrm{r}}$	(3.47)
Third thermal virial coefficient			
$C(T) = \frac{1}{2}\lim_{\rho\to 0}\left(\frac{\partial^2\left(\frac{p}{\rho RT}\right)}{\partial\rho^2}\right)_T$	(3.48)	$C\rho_{\mathrm{r}}^2 = \lim_{\delta\to 0}\alpha_{\delta\delta}^{\mathrm{r}}$	(3.49)

4 Fitting Equations of State

Fitting generally means adjusting parameters of a given functional form, which are exponents, coefficients, and other parameters of equations of state, to approach the underlying experimental data in the best possible way. In this work, the fundamental equation of state is expressed in terms of the Helmholtz energy as a function of temperature and density.

Reducing flexibility of the functional form, such as limiting the number of terms, ensures a suitable physical behavior and reasonable extrapolation. In order to get a highly accurate equation of state, it is of importance to use different properties in a broad range of temperature and pressure. The quality of the used data sets is most important, since this is the most important condition for quality and accuracy of the developed equation of state, which should represent all underlying data within their experimental uncertainties. Since measurements are difficult to carry out for very high or low temperatures and pressures and usually around the critical point, constraints ensure correct physical extrapolation of the equation of state.

All of the parameters of equations of state are adjustable. To maintain the correct physical behavior of equations of state, the influence of each parameter is of major interest for the correlator, as well as the consideration of rough guidelines for temperature and density exponents. Temperature exponents, as discussed in section 3.2.2, do not necessarily have to be integer values, but should remain positive. Density exponents are restricted to positive integers, since derivatives with respect to density have to vanish for $\rho \to 0$, which represents an ideal gas with no molecular interaction. Non-integer exponents on density would result in an infinite value at zero density for certain derivatives of pressure. Since the viral expansion

$$\frac{Z-1}{\rho} = B + C\rho + D\rho^2 + \cdots, \tag{4.1}$$

derived from Eq. (3.5) represents the correct transition from ideal gas to real gas behavior, the density exponents are directly related to the virial coefficients. The viral expansion in Eq. (4.1) is shown in Figure 4.1.

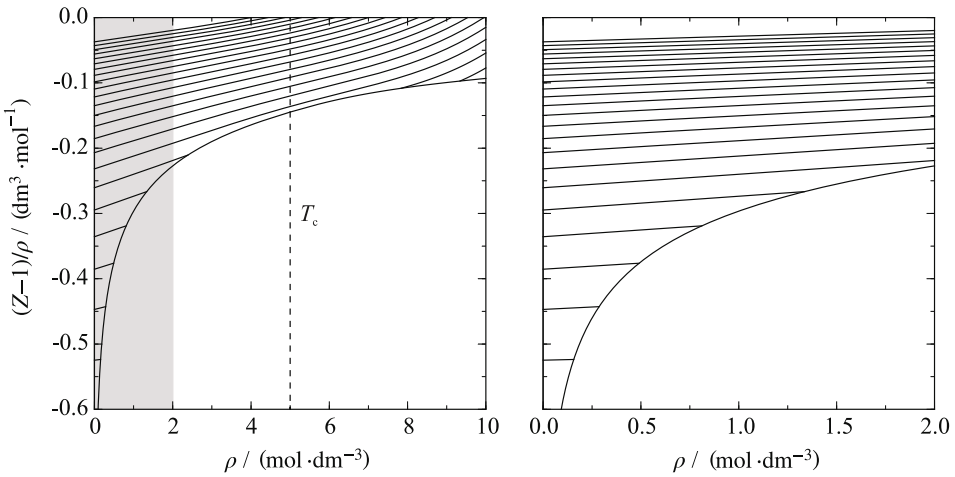

Figure 4.1 Left: $(Z-1)/\rho$ as a function of density for selected isotherms in the range from 100 K to 700 K for propane. Right: Higher resolution of the grey marked area in the left plot. Figure according to Thol (2015).

The second virial coefficient B represents the intercepts with the ordinate, the third virial coefficient C is the slope, and the fourth coefficient D determines the curvature of the virial expansion in Eq. (4.1) and Figure 4.1. While approaching ideal gas behavior ($\rho \to 0$), the contribution from the third and fourth viral coefficients is negligible. Higher virial coefficients can be used to represent the fluid in the higher density region and with sufficiently high coefficients, even the liquid behavior can be modeled. The final equation of state has to have at least one term with density exponents of one, two, and three, representing the virial coefficients B, C, and D, respectively, to ensure the correct transition from ideal gas to real gas behavior.

In the following, the fitting procedure is explained and presented in further detail. Fitting algorithms for developing equations of state can roughly be categorized as linear and non-linear procedures. The difference between them is the way how experimental data are used and correlated by least-squares fitting.

The advantage of nonlinear fitting is the ability to use all properties as an input, without any transformation, whereas with linear fitting, preliminary equations are needed to obtain the independent variables of density and temperature from measured properties such as pressure and temperature. Nonlinear fitting procedures also benefit by being able to more easily control the extrapolation behavior and two phase behavior, since inequality criteria can be used. Nonlinear algorithms are able to control the shapes of equations of state with the use of inequalities to compare expected behavior against how the current equation is behaving. Linear fitting procedures often involve extrapolation by hand and a manual determination of data points to yield the right shape. The fitting approach determines how the adjustable parameters of the equation

of state are obtained by the method used to reduce the overall sum of squares of the deviations of calculated properties from the input data. The nonlinear approach uses the equation

$$\mathrm{SSQ} = \sum_{i=1}^{I} W_{\rho,i} F_{\rho,i}^2 + \sum_{j=1}^{J} W_{p,j} F_{p,j}^2 + \sum_{k=1}^{K} W_{w,k} F_{w,k}^2 + \cdots. \tag{4.2}$$

In Eq. (4.2), W_x is the weight for each data point of the thermodynamic property x as selected by the person implementing the fit. The deviation F_x is defined by

$$F_x = \frac{x_{\mathrm{Data}} - x_{\mathrm{EOS}}}{x_{\mathrm{Data}}}. \tag{4.3}$$

The sum of squares is a convenient benchmark used to evaluate the representation of all fitted data points and constraints by the current equation of state.

The weight on each data point controls the contribution of that point to the fit. The absolute value is not an appropriate scale to evaluate the quality of the equation of state with respect to the underlying data sets. The more important issue in setting the individual data weights is considering experimental or statistical uncertainty of each weighted data point, as well as the type of thermodynamic property. Furthermore, property measurements, for instance in the critical region or at phase boundaries, yield different kinds of uncertainties. The correlator should pay attention to the source of data, which can be estimated from simulations or obtained from measurements. Hence, quality of data are highly dependent on either the chemical model used to approach the real behavior of the compound or the apparatus used to measure each type of property.

During the fitting process, the correlator needs to consider the deviation output, displaying relative and weighted deviations of each data point of a property, as well as the constraints used. This gives an idea of the quality of the fitted equation of state at that point in time, and how the data are represented by the equation. With close understanding of the uncertainties of each data point, setting higher weights forces the fitting procedure to more closely match particular data points.

The quality of equations of state is also assessable by investigating thermodynamic diagrams. Those can be obtained from REFPROP (REFerence Fluid PROPerties) by Lemmon *et al. (*2018), a program used for calculating thermodynamic and transport properties of fluids. The 2018 released version 10.0 of REFPROP includes 147 pure fluids. When the current equation

of state is added, REFPROP can show thermodynamic diagrams from that equation. Although underlying data can be represented correctly by the equation of state, it might still fail close to phase boundaries or in the critical region due to incorrect physical behavior. Incorrect behavior can be easily detected by unreasonable shapes of the thermodynamic diagrams, for instance by abrupt changes in isotherms or missing saturation lines in the critical region. Consequently, both deviation plots of data points and thermodynamic diagrams must be considered. Weighting constraints helps to control extrapolations by creating barriers for slopes, curvatures, or even higher deviations, and by shaping the isotherms or saturation lines to their correct form. The problem in setting constraints to obtain a specific shape lies within the prediction of supposedly correct behavior of thermodynamic properties for the particular fluid being fitted in regions where no experimental data are available. To predict certain behavior of properties, the correlator requires a well-developed reference equation of state of a comparable fluid, which reveals similar chemical behavior and structure. This requirement was one of the most challenging aspects in this work because the physical behavior of propylene glycol significantly differs from the behavior of other well-known fluids due to its special chemical characteristics, cf. Section 2.

A quantity that can be used to confirm the correct extrapolation behavior are ideal curves. Along ideal curves one property of the real fluid is equal to the corresponding property of the hypothetical ideal gas. Ideal curves are usually shown in reduced logarithmic temperature and pressure diagrams, as demonstrated in Figure 4.2. For simple molecules, the Boyle curve, Ideal curve, Joule-Thomson curve, and sometimes even the Joule inversion curve lie within regions where experimental data are available. This is not the case for more complex molecules with higher critical temperatures, as for propylene glycol, due to the strong association character. Thus, the basic shape is determined by extrapolations and gives a reasonable idea of the quality of the equation of state. The limited range of experimentally available data for propylene glycol and for comparison also for pentane and methane are shown in Figure 4.2. The pressure range of propylene glycol is determined excluding the high-pressure measurements of Bridgman (1932) (see section 5.6).

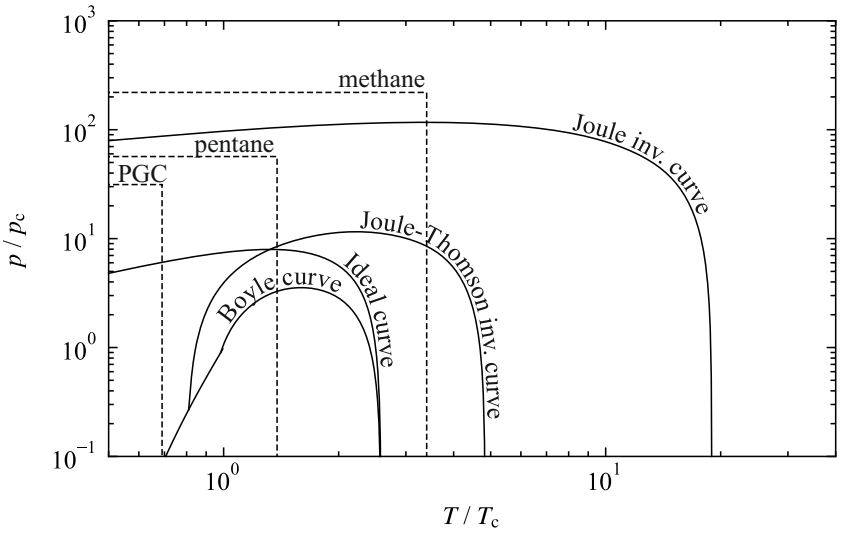

Figure 4.2 Typical plot of the considered ideal curves for the truncated and shifted Lennard-Jones model in a reduced double-logarithmic pressure and temperature diagram according to Thol *et al.* (2015). Ranges of available data for propylene glycol (PGC), pentane, and methane are included. PGC data range without consideration of data obtained by Bridgman (1932).

Comparing with existing equations of state for other fluids with similar chemical properties and extrapolation behavior is the best method to determine how the fitted fluid is performing. Even more important is to find a suitable fluid with a well-developed equation of state for use as the starting point in the development of the new equation of state. For propylene glycol, the equation of state of ethylene glycol by Zhou and Lemmon (2018) with 21 terms (seven polynomial, seven exponential, and seven GBS terms) was used.

5 The Equation of State for Propylene Glycol

In this chapter, the fundamental equation of state in terms of the Helmholtz energy of propylene glycol is presented, as well as the ancillary equations used for calculations at vapor-liquid boundaries. To illustrate the accuracy of the equation of state, calculated property values are compared to the experimental data, with a closer look at the underlying data sets, to which the equation of state was fitted. The extrapolation behavior of the final equation of state is also evaluated with an analysis of the shape of thermal and caloric properties and ideal curves.

5.1 Data Analysis

Before starting the fitting process to develop the equation of state, all data sets need to be acquired from the literature, optimally covering the fluid state over a broad temperature and pressure range. In order to find publications containing properties of propylene glycol, the databank *Thermo Data Engine (TDE)* of the *National Institute of Standards and Technology* was used and supplemented by a comprehensive literature research. All data sets were converted to the ITS-90 scale and SI- units. In the process of fitting, an appropriate quantity and quality of the applied data maintains flexibility and accuracy of the equation of state. Consequently, the correlator has to choose data sets considering their measurement uncertainties, influence on other data sets, and range of fluid states covered.

The defined percent deviation of any measured or estimated data point x_{Data} from the calculated property x_{EOS} is

$$\Delta x = 100\left(\frac{x_{\mathrm{Data}} - x_{\mathrm{EOS}}}{x_{\mathrm{Data}}}\right). \tag{5.1}$$

Data should ideally be represented within the measurement uncertainties. A more convenient quantity to compare data sets from different sources with respect to their deviations from the equation of state is the averaged absolute relative deviation (AAD):

$$\mathrm{AAD} = \frac{1}{N}\sum_{i=1}^{N}|\Delta x_i|. \tag{5.2}$$

In Eq. (5.2), the quantity N corresponds to the number of data points for each author and property.

The available data found for developing the equation of state for propylene glycol are included in 164 publications with measured data as well as estimated values by group contribution methods. Altogether, 1357 data points were included, comprising homogeneous densities, vapor pressures, isobaric heat capacities, speed of sound, and critical point data. A summary of all data points and the actual quantity of fitted data points is given in Table 5.1.

Table 5.1 Summary of all underlying and experimental data points.

Property	All available data points	Fitted data points
c_p	18	5
c_p^{o}	estimated data from correlations	3
$p\rho T$	885	31
p_{v}	245	13
w	208	21
Total	1357	73

In order to ensure a stable and physically correct behavior of the equation of state, the underlying data sets need to represent the fluid state in a broad temperature and pressure range. The measurement techniques, the purity of the sample, and the uncertainty of the apparatus employed is of great importance. The quality of data sets are closely related to the quality and the reliability of the equation of state. Ideally, reliable and reasonable uncertainties of the measured quantities are given by the author and can be included in the fitting procedure. Unfortunately, older publications usually lack a quantification of measurement uncertainties, but are not significantly less likely to contain high quality data. To state the unknown combined uncertainties of measurements, all relevant factors need to be taken into account. Only researchers with comprehensive knowledge of the apparatuses used and measurement techniques are able to analyze the particular uncertainty factors in the measurement.

5.2 Estimation Methods and Critical Point Considerations

Due to the limited range of density measurements, the fluid state of homogeneous density at high temperatures and within a relatively wide range below the critical temperature at 676.4 K, which is measured by VonNiederhausern *et al.* (2000), is not represented by experimental data. The reason for this gap in experimental data is the thermal decomposition of propylene glycol.

Propylene glycol already decomposes due to oxidation reactions at modest temperatures of 400 K to 600 K into acetone, acetaldehyde, formaldehyde, and carbon dioxide via carbon bound cleavage according to Diaz *et al.* (2010). Even at lower temperatures, some dissociation can be expected.

Consequently, the critical properties are difficult to obtain with conventional measurement techniques. Nonetheless, a flow method has been developed by VonNiederhausern *et al.* (2000) in order to obtain reliable critical data for thermally unstable compounds like propylene glycol. Static, conventional measurements of critical data usually achieve higher accuracy, but can not be applied to compounds that are not stable at their critical point. The flow method by Von-Niederhausern *et al.* (2000), slightly changed with respect to an earlier method by Wilson *et al.* (1995), is presented. In order to measure critical temperatures of a thermally unstable compound with a static method requires an unreasonably fast heat up rate of the sample to avoid thermal decomposition. Usually, the heat capacities of heater and sample container interfere with a rapid heat up. With the flow method, short residence times avoid thermal decomposition, but also demand a high heating rate to reach the critical temperature of the sample passing through the tube. Ideally, heat up time and fluid flow rate should be the same. To comply with the above mentioned conditions, capillary tubing is used to ensure undisturbed heating of fluid elements, almost without any storage of heat within the material. Figure 5.1 shows a detailed scheme of the flow apparatus.

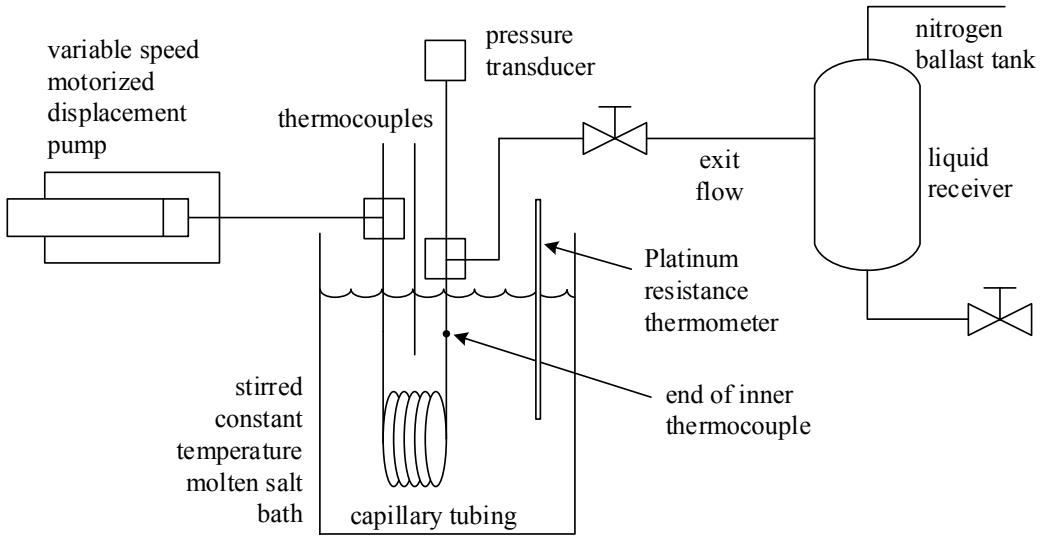

Figure 5.1 Schematic of the flow apparatus for measuring the critical temperature and the critical pressure according to VonNiederhausern *et al.* (2000).

The advantage of this measurement technique is that accurate temperature scans can be taken in a wide time frame, since the temperature bath can be heated smoothly at very low residence times of the samples. To obtain the critical temperature and pressure, several temperature scans close to the critical point need to be evaluated. A single, sub critical temperature scan is characterized by a flat, horizontal region, indicating isothermal boiling at constant pressure, followed by slowly increasing the bath temperature. This behavior does not exist above the critical point, where the transition between liquid and gas is indiscernible. Evaluation of several temperature scans at different pressures show a narrow region for the critical temperature at a given pressure. Thus, the critical point is inferred by the temperature and pressure where isothermal boiling is no longer observed and, therefore, accompanied with several tenth of Kelvin uncertainties due to errors in interpretation. Uncertainty is also caused by impurities and fluctuating flow rates of the samples. A few measured series at varying, averaged residence times provide a convenient basis for a quadratic extrapolation to zero residence time, which gives the actual critical temperature of the compound. Taking the uncertainty of extrapolation into account, the overall errors for temperature and pressure are 1 K and 2 %, respectively. The uncertainties of critical point measurements for propylene glycol are essentially smaller with values of 0.3 K and 0.007 MPa according to VonNiederhausern *et al.* (2000). Thus, the flow method yields sufficiently accurate critical data, where other methods fail. The critical temperature and pressure were finally measured at 676.4 K and 5.941 MPa. Due to the fact that data are obtained with a flow method, the measurement of critical density is not possible. VonNiederhausern *et al.* (2000) provides no explanation for the much smaller assumed uncertainty in the measurement of the critical parameters of propylene glycol compared to the overall estimated uncertainty of the flow method.

The difficulty is to get close to the critical point in the first place. If no reliable measured data of critical properties are available from other measurements, estimations from group contribution methods can also be taken into account. The most established method, which is still applicable for a broad field of compounds, is the method of Joback (1984), which is based on an earlier group contribution method of Lydersen (1955). Other group contribution methods, e.g., by Constantinou and Gani (1994), Wilson and Jasperson (1996), or Marrero and Pardillo (1999) differ slightly in terms of group and bond consideration or normal boiling point estimation according to Poling *et al. (*2001). The method of Joback distinguishes between ring and chain elements of molecules and takes the difference between alcoholic and phenolic hydroxyl groups into account. Contributions of each group are summed, multiplied by the number of occurrences

in the molecule and included in the estimation scheme of Joback. Unlike Joback's method, the one by Marrero and Pardillo is more a group interaction method, while Wilson and Jasperson also consider atomic contributions. Despite the variability in considering different contribution factors, all methods are broadly applicable for the selected substances (Poling *et al.* (2001) Appendix A) and are roughly comparable in accuracy. The error for the critical temperature for most of the substances is around 1 %. The critical pressures usually have errors around 5 % according to Poling *et al. (*2001). Generally, accuracy is higher for smaller molecules and by using experimental data for the normal boiling point in the critical temperature estimation. However, the suitability of these three group contribution methods needs to be closely reviewed when considering critical data for propylene glycol. Propylene glycol is considered to be a strongly associating substance, which forms cluster of several molecules due to hydrogen bonds. Since group contribution methods only consider the effect of groups and their interactions, they might not be suitable to estimate critical properties of associating substances. In fact, the critical temperature of propylene glycol, estimated by the method of Joback, is 626 K, which is roughly 50 K below the measured temperature of VonNiederhausern *et al.* (2000). The estimated critical pressure is 6.1 MPa, 0.159 MPa higher than the measured value of VonNiederhausern *et al.* (2000). A different approach for estimating critical data is used by the Quantitative Structure-Property Relationships (QSPR) methodology, which is often combined with the Support Vector Machines (SVM) regressions. The idea is to relate the property of interest to molecular features derived theoretically from the chemical structure of the compound. The connection between properties and descriptors, is built by regression analysis through the use of large collections of data according to Kazakov *et al.* (2010). However, estimated critical data are not considered within the fitting procedure due to the difficulties mentioned above in obtaining data for propylene glycol.

There are no data for the isobaric heat capacity of the ideal gas for propylene glycol. The Joback group contribution method according to *VDI Wärmeatlas* (2013) was used, to obtain an estimate of the data range. The isobaric heat capacity of the ideal gas consists of two major contributions: the temperature independent part, representing the translatational and rotational energy, and the temperature dependent part, considering vibrational energy of the molecule (see section 3.2.1). Joback's equation is defined by a constant and three temperature dependent polynomial terms (see *VDI Wärmeatlas* (2013)):

$$\frac{c_p^\circ}{\mathrm{J/(kg \cdot K)}} = A + B\frac{T}{\mathrm{K}} + C\left(\frac{T}{\mathrm{K}}\right)^2 + D\left(\frac{T}{\mathrm{K}}\right)^3. \tag{5.3}$$

The coefficients A, B, C, and D are estimated in terms of group contributions of propylene glycol. As for the critical data estimation, it is expected that Joback's group contribution method is not suitable for propylene glycol, since the associative nature of propylene glycol is not taken into account. To underline this assumption, the vibrational behavior of propylene glycol molecules is more closely examined, since the vibrational energy part contributes with three polynomial term to equation (Eq. 5.3). Ahlström *et al.* (1998) investigated the vibrational density of state (DOS), taken from molecular dynamic simulations, for propylene glycol. From this, the behavior of frequency bands in different ranges and for different chain length of propylene glycol molecules were evaluated. Ahlström *et al.* (1998) used chains of 1, 2, and 45 molecules for their investigation. The low frequency band (below 600 $\mathrm{cm^{-1}}$) reveals a clear peak at 50 $\mathrm{cm^{-1}}$, which is insensitive to chain length and group interactions within the chain. Nevertheless, the peak increases in relative intensity for decreasing molecular size according to Ahlström *et al.* (1998). Thus, the low frequency band can be considered to represent the intermolecular vibration or the degrees of freedom of the different chains. Propylene glycol appears to have non-negligible vibration energy because of its association, which is not reducible to only group interactions. Although Joback's method is predicted to have deviations of only 1 % to 2 % for small molecules according to *VDI Wärmeatlas* (2013), the method is unlikely to yield suitable ideal isobaric heat capacity data for propylene glycol.

In the course of new software implementations and model developments of the Thermo Data Engine (TDE), a modified equation for the estimation of the ideal isobaric heat capacity with revised parameters and ring contributions has been developed by Diky *et al.* (2013). Although, the most recent progress in predicting ideal isobaric heat capacity data for associating fluids is not published yet, the participating authors for the TDE software development can be found in Diky *et al.* (2013). The conventionally estimated Joback data and the data obtained from the improved equation for the ideal heat capacity by Diky *et al.* (2013) are presented in Chapter 5.3 in Figure 5.2.

5.3 Ideal Part of the Equation of State

The ideal part of the equation of state is represented by the isobaric heat capacity of the ideal gas. The ideal-gas isobaric heat capacity is defined with respect to the Planck-Einstein terms (Eq. (3.22)). Further, the Helmholtz energy of the ideal gas can either be formulated in combination with polynomial terms, as it is derived in chapter 3.2.1 and presented in Eq. (3.25), or without additional polynomial terms. With latter considerations, the ideal part of the equation of state for propylene glycol can be written as

$$a^{\circ}(\tau,\delta) = c^{\mathrm{II}} + c^{\mathrm{I}}\tau + 3\ln(\tau) + \ln(\delta) + \sum_{i=1}^{3} m_i \ln[1-\exp(-\theta_i\tau)]. \qquad (5.4)$$

The two integration constants can be calculated to $c^{\mathrm{I}} = -2.623045468964$ and $c^{\mathrm{II}} = 7.665655773743$. The parameters of the Planck-Einstein terms in Eq. (5.4) are listed in Table 5.2.

Table 5.2 Parameters of the Planck-Einstein terms of the ideal part of the equation of state according to Eq. (5.4).

i	m_i/-	θ_i/K
1	4	0
2	3.4	850
3	410	1500

The estimated ideal-gas isobaric heat capacity data are compared with respect to their deviations from the equation of state. Figure 5.2 shows the percentage deviations of the estimated data points by Joback and the modified equation by Diky *et al.* (2013). All deviations are shown within the range of validity of the equation by Diky *et al.* (2013) from 200 to 1000 K. At this time of investigation, it cannot be stated, wether the large deviations are due to the insufficiently represented ideal part of the equation or to an inappropriate estimation method of the ideal-gas isobaric heat capacity data. Therefore, the parameters were mainly fitted to reliable speed of sound data in the liquid state instead of the estimated isobaric heat capacity data of the ideal gas.

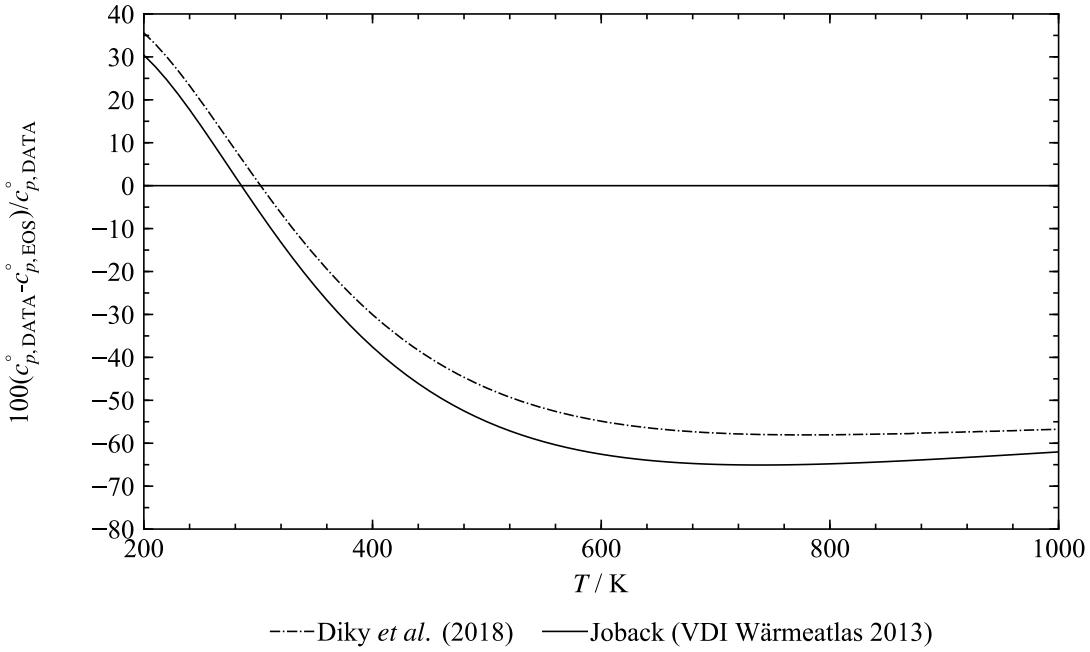

Figure 5.2 Deviations of the modified ideal-gas isobaric heat capacity equation by Diky *et al.* (2018) and the estimated Joback data points (*VDI Wärmeatlas* (2013)) from the equation of state.

5.4 Residual Part of the Equation of State

The residual part of the equation of state for propylene glycol consists of seven polynomial, seven exponential, and six Gaussian bell-shaped (GBS) terms. Thus, the equation (3.26) can be specified to

$$\begin{aligned}\alpha^{\mathrm{r}}(\tau,\delta) = &\sum_{i=1}^{7} n_i \tau^{t_i} \delta^{d_i} + \sum_{i=8}^{14} n_i \, \tau^{t_i} \delta^{d_i} \exp(-\gamma_i \delta^{p_i}) \\ &+ \sum_{i=15}^{20} n_i \, \tau^{t_i} \delta^{d_i} \exp(-\eta_i (\delta - \varepsilon_i)^2 - \beta_i (\tau - \gamma_i)^2).\end{aligned} \tag{5.5}$$

Most of the fluid states are covered by the exponential and polynomial terms. The critical region is represented by a fairly high number of GBS terms, which is usually kept in a range of three to five. All parameters of Eq. (5.5) are listed in Table 5.3.

Table 5.3 Parameters of the residual part of the equation of state according to Eq. (5.5).

i	n_i	t_i	d_i				
1	0.034647478	1	5				
2	–2.0876981	1.198	1				
3	–0.18393678	0.9199	4				
4	0.49152392	0.627	3				
5	–1.8119252	1.1911	2				
6	3.649855	0.1378	1				
7	–2.5971548	0.325	1				
i	n_i	t_i	d_i	p_i			
8	–0.002127152	2.0666	7	1			
9	1.964417	1.015	2	1			
10	0.19412219	1.531	6	1			
11	4.026081	1.4564	3	1			
12	0.94976352	1.443	4	1			
13	–2.4910022	1.681	3	1			
14	–0.12726899	1.9578	5	1			
i	n_i	t_i	d_i	η_i	β_i	γ_i	ε_i
15	–1.6470116	1	3	20	1000	1.09	0.93
16	0.15910207	2.3	1	2.66	1.13	2.06	1.72
17	0.20622381	1.97	1	2.5	1.99	1.28	1.45
18	–0.090452877	0.77	2	1.157	1.12	0.969	0.6824
19	–0.055164609	2.6	3	3.1	1.5	2.24	1.53
20	–0.12328159	2.57	4	2.1	0.365	2.245	1.0568

Considering all underlying data, the range of validity can be determined by the triple point temperature T_{tr} = 214 K and the upper temperature and pressure limits covered by the data set of Sagdeev *et al.* (2017). The maximum temperature and pressure are $T_{\max}$ = 452 K and $p_{\max}$ = 245 MPa. Bridgman (1932) yields density measurements at perspicuously higher pressures up to 1177 MPa. The data by Bridgman (1932) are not considered in the fitting process; anyhow, the equation of state shows an appropriate extrapolation behavior to fairly high pressures, which is discussed in more detail in chapter 6.

5.5 Ancillary Equations

The equations for the vapor pressure p_v, the saturated liquid density ρ', and the saturated vapor density ρ'' are ancillary equations used to estimate starting values for the iterative calculation of properties along the saturation line. Thus, the fitting process of the equation of state is expedited perceptibly. The parameters of Eqs. (5.6) to (5.8) are listed in Table 5.4.

$$\ln\left(\frac{p_\mathrm{v}}{p_\mathrm{c}}\right) = \frac{T_\mathrm{c}}{T}\sum_{i=1}^{5} n_i \left(1-\frac{T}{T_\mathrm{c}}\right)^{k_i} \tag{5.6}$$

$$\frac{\rho'}{\rho_\mathrm{c}} = 1 + \sum_{i=1}^{N} n_i \left(1-\frac{T}{T_\mathrm{c}}\right)^{k_i} \tag{5.7}$$

$$\ln\left(\frac{\rho''}{\rho_\mathrm{c}}\right) = \sum_{i=1}^{N} n_i \left(1-\frac{T}{T_\mathrm{c}}\right)^{k_i} \tag{5.8}$$

The deviations of the ancillary equations from the equation of state are shown in Figure 5.3. For a broad temperature range, starting at the triple point temperature T_tr = 214 K and close to the critical temperature T_c = 676.4 K, the deviations are within 0.05 %, except for the density of saturated vapor, which exhibits slightly higher deviations at lower temperatures.

Table 5.4 Parameters of the ancillary equations for the vapor pressure p_v, the saturated liquid density ρ' and the saturated vapor density ρ'' according to Eqs. (5.6) to (5.8).

	p_v, Eq. (5.4)		ρ', Eq. (5.5)		ρ'', Eq. (5.6)	
i	n_i	k_i	n_i	k_i	n_i	k_i
1	–9.648	1	4.554	0.66	–0.2938	0.1
2	1.9322	1.5	0.5124	0.16	–52.614	4.637
3	–0.08408	0.05	–5.308	1.114	–5.9348	0.6
4	–6.1415	3.038	3.832	1.61	–15.99	2.01
5	–10.781	11.766	–1	2.19	–421.2	20.865
6					–131.3	10.412

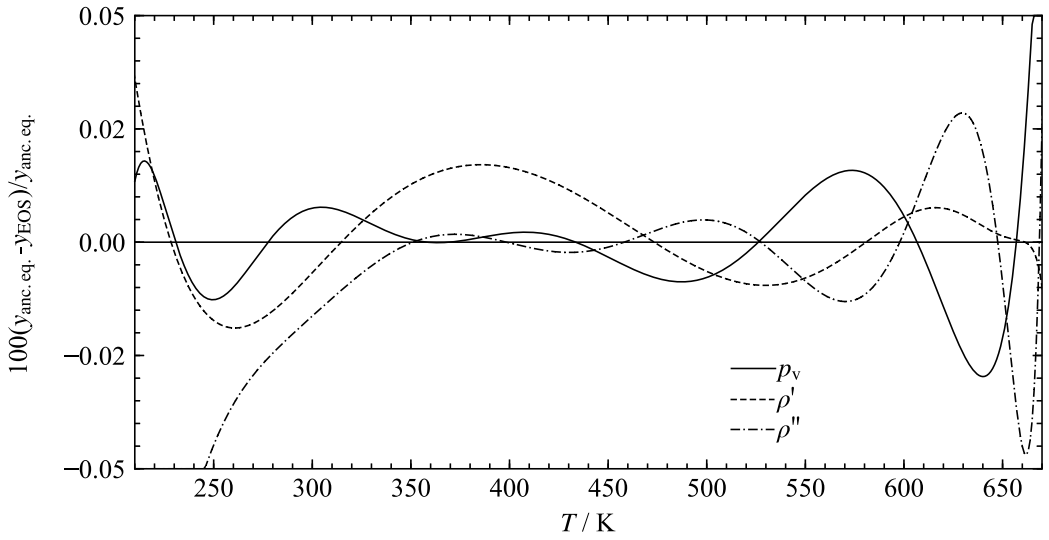

Figure 5.3 Deviations of the ancillary equations for the vapor pressure and the saturated liquid and vapor density from the equation of state.

5.6 Comparison of Single Phase Density Data

All underlying single phase density data sets for propylene glycol are listed in Table 5.5 along with their temperature and pressure ranges and the average absolute relative deviations (AAD).

Table 5.5 Summary of all underlying single phase density data along with the temperature and pressure ranges and their average absolute relative deviations (AAD) with respect to the equation of state.

Authors	Data points	*T*/K	*p*/MPa	AAD/%
Atilhan and Aparicio (2013)	126	278 - 358	0.1 - 60	0.027
Bajić *et al.* (2013)	10	288 - 333	0.101325	0.019
Bridgman (1932)	42	273 - 368	0.098 - 1180	0.87
Curme *et al.* (1952)	41	273 - 313	0.101325	0.020
Domańska *et al.* (2014)	9	313 - 353	0.101325	0.022
Garber *et al.* (1970)	5	293.15	0.101325	0.15
George and Sastry (2003)	5	298 - 338	0.101325	0.022
Geyer *et al.* (2000)	5	278 - 318	0.101325	0.065
Geyer *et al.* (2001)	12	288 - 308	0.1 - 60	0.045
Guignon *et al.* (2010)	8	288.30	0.1 - 349	0.16
Jiménez and Martinez (2006)	5	293 - 313	0.101325	0.023
Khattab *et al.* (2013)	7	293 - 323	0.101325	0.26
Krishna *et al.* (2015)	6	298 - 323	0.101325	0.031
Li *et al.* (2007)	8	298 - 333	0.101325	0.05
Li *et al.* (2008)	8	293 - 328	0.101325	0.039
Ling *et al.* (2011)	6	298 - 323	0.101325	0.038

Authors	Data points	T/K	p/MPa	AAD/%
Ling *et al.* (2016)	6	293 - 318	0.101325	0.046
Makarov *et al.* (2016)	15	274 - 333	0.101325	0.037
Marchetti *et al.* (2000)	19	263 - 353	0.101325	0.025
Nain (2007)	6	293 - 318	0.101325	0.056
Olson and Cordray (1992)	7	273 - 418	0.101325	0.063
Pal *et al.* (2016)	6	293 - 318	0.1	0.037
Ponedelnikova and Tarasova (1954)	12	258 - 363	0.101325	0.077
Rane *et al.* (2016)	6	293 - 318	0.095	0.025
Romero *et al.* (2008)	6	283 - 308	0.099	0.037
Sadykov *et al.* (1974)	16	303 - 453	0.101325	0.21
Sagdeev *et al.* (2017)	57	293 - 452	0.098 - 245	0.21
Saleh *et al.* (1999)	5	303 - 323	0.101325	0.079
Soldatović *et al.* (2016)	7	293 - 323	0.1	0.024
Sun and Teja (2004)	8	299 - 440	0.1 - 2.2	0.15
Timmermans and Hennaut-Roland (1955)	7	273 - 303	0.101325	0.025
Tsai *et al.* (2009)	5	303 - 343	0.101325	0.055
Vinogradov and Shakhparonov (1984)	7	243 - 333	0.101325	0.043
Sampson *et al.* (2018)	100	273 - 393	5.01 - 91.4	0.018
Zander (1882)	9	288 - 451	0.101325	10.5
Zarei *et al.* (2008)	7	293 - 343	0.082	0.023
Zarei *et al.* (2013)	6	293 - 333	0.101325	0.022
Zemánková *et al.* (2013)	5	283 - 313	0.101325	0.037
Zhuravlev (1992)	19	243 - 423	0.101325	0.22
Zhuravlev *et al.* (1985)	15	223 - 363	0.101325	0.1
Zivković *et al.* (2014)	8	288 - 323	0.101325	0.018
Zorebski *et al.* (2008)	73	283 - 363	0.1 - 100	0.012
All authors with fewer than five data points	145	273 - 358	0.001 - 0.101	0.14
Overall	885	223 - 453	0.082 - 1180	

The single phase region of propylene glycol is relatively well covered by density measurements around ambient pressure and temperature. All data are within a range of 223 K to 453 K and 0.001 MPa to 1180 MPa and, hence, cover a broad pressure range including values at very high pressures such as in the measurements by Bridgman (1932). The density measurements by Sadykov *et al.* (1974) reach the highest value in temperature of 453 K. Fitted data sets as well as the above mentioned data obtained by Bridgman (1932) and Sadykov *et al.* (1974) are presented in Figure 5.4.

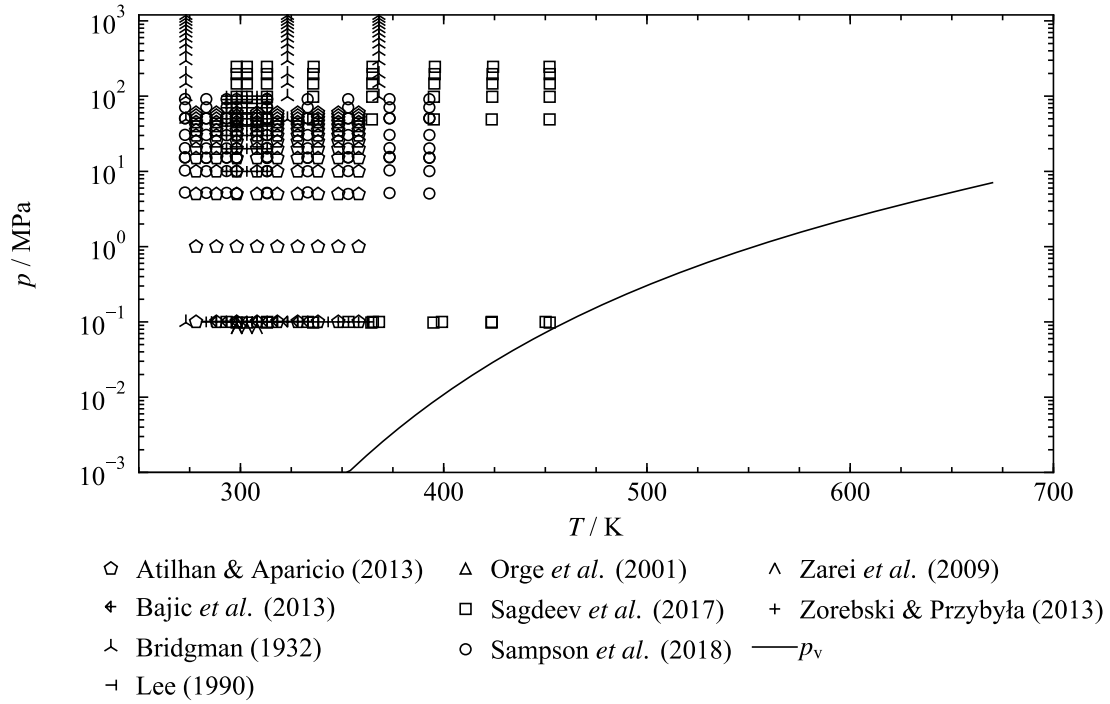

Figure 5.4 Pressure as a function of temperature of selected density data in relation to the vapor pressure curve.

The data of Sampson *et al.* (2018) cover a temperature range of 273 K to 393 K and reach pressures up to 91 MPa. The set includes 100 density data points in the liquid phase and is, thus, the second comprehensive data set. The measurements of Sampson *et al.* (2018) were carried out with a commercial high pressure vibrating-tube densimeter (VTD) of the type DMH HPM manufactured by Anton Paar. The vibrating-tube measurement is based on the relation between the density and the vibration period of a U-shaped tube, which is detected by an optical sensor according to Kayukawa *et al.* (2003). Before the measurement, the VTD was calibrated at temperatures between 283 K and 383 K with pressures up to 98 MPa. The substances used for the calibration were water and helium, which are typical compounds for this purpose. The density of water is extremely well represented by the equation of state of Wagner and Pruss (2002) over a wide region. The liquid-phase density of propylene glycol and water are similar, whereas helium is used as a fix point at comparatively low densities. Using two underlying models of Outcalt and McLinden (2007) and May *et al.* (2014), a very accurate correlation is obtained. Yang estimated the relative combined expanded uncertainty to be within 0.15 % (1.56 kg·m^{-3}), considering temperature, pressure, and oscillation period estimations, as well as sample impurities of 99.5 mol-% for a degassed sample and uncertainties due to the calibration. Each single data point is represented by the equation of state with a deviation of 0.06 %, which is within

their measurement uncertainties (0.15 %). In fact, the uncertainty estimate seems to be very conservative and might be reduced to at least 0.1 %.

Furthermore, the data set of Zorebski and Przybyła (2013) includes 73 data points in a temperature range of 283 K to 363 K and up to fairly high pressures of 100 MPa. The data set contains single point measurements at ambient pressure for temperatures between 318 and 363 K, as well as for temperatures of 283 K and 288 K. In the range of 293 K to 313 K, densities were measured for pressures between 0.1 MPa and 100 MPa in steps of 10 MPa. The densities were measured on a 99.5 mol-% pure sample with a vibrating-tube densimeter (DMA 5000 Anton Paar), which is provided with automatic viscosity correction. The calibration was carried out with air and re-distilled, deionized, and degassed water. Zorebski and Przybyła (2013) claim a fairly small uncertainty of 0.018 $kg \cdot m^{-3}$, which is obtained from an average value. The deviation of the data from the equation of state are within 0.04 % over the entire temperature and pressure range. The measured densities of Zorebski and Przybyła (2013) are in a very good agreement with those obtained by Zarei *et al.* (2009) and Orge *et al.* (2001), but not with the data of Lee (1990). Zarei *et al.* (2009) followed the hypothesis that the discrepancy with the data of Lee (1990) is related to the missing viscosity correction in the measurement procedure. This observation can be validated by taking deviations from the equation of state into account. The three data points of Zarei *et al.* (2009), containing measurements at 298 K, 303 K, and 308 K at 0.1 MPa, show deviations smaller than 0.07 %, very close to the deviations of Zorebski and Przybyła (2013) in the corresponding temperature and pressure range. In fact, the deviations of Zorebski and Przybyła (2013) and Zarei *et al.* (2009) differ by 0.006 percentage points and thus the good agreement is corroborated. The data obtained by Zarei *et al.* (2009) were measured with an Anton Paar DMA 4500, which also uses an automatic viscosity correction. With a 99.5 mol-% propylene glycol sample, their estimated uncertainty is smaller than $1 \cdot 10^{-5}$ $g \cdot m^{-3}$. One mentioned data point by Orge *et al.* (2001) is closer than 0.005 percentage points to the corresponding data point measured by Zorebski and Przybyła (2013), which supports the good agreement of those independent data sets. Also the discrepancy of the measured data by Zarei *et al.* (2009) with the data set of Lee (1990) is shown by the deviations from the equation. The deviations of data points at ambient pressure and 293 K differ by more than 0.06 percentage points. The data set of Bajić *et al.* (2013)is independent to the one of Zorebski and Przybyła (2013) and shows conforming data points within a temperature range of 288 K to 333 K at a pressure of 0.1 MPa. Bajić *et al.* (2013) used exactly the same measurement apparatus and calibration procedure, while claiming even smaller measurement uncertainties of 0.01 $kg \cdot m^{-3}$.

The data sets of Zorebski and Przybyła (2013) and Bajić *et al.* (2013) are supported by the data set of Atilhan and Aparicio (2013), which, with 126 data points, is the largest data set. The measurements were obtained over a large temperature range of 278 K to 358 K for pressures between 0.1 MPa and 60 MPa. A 99.99 mass-% sample was used in an automated Anton Paar DMA 512P vibrating-tube densimeter with a high pressure cell. The densities were correlated with the TRIDEN 10-parameter Ihmels and Gmehling equation of state Ihmels and Gmehling (2001). Furthermore, Atilhan and Aparicio (2013) used n-hexane and water as reference fluids together with a 14-parameter equation for calibration purposes. The uncertainty of the experimental density data is estimated to be smaller than 0.0012 g·cm^{-3} (0.11 %), which is noticibly higher than the claimed uncertainties of the above compared data sets by Zorebski and Przybyła (2013) and Bajić *et al.* (2013). The higher uncertainty is likely to be related to the missing viscosity correlation. Referring to the analysis of the viscosity-induced errors on vibrating-tube density measurements by Sanmamed *et al.* (2007), Atilhan and Aparicio (2013) estimated the uncertainty related to viscosity to be smaller than 0.0005 g·cm^{-3} for viscosities below 200 mPa·cm. Taking the uncertainty limit of 0.0012 g·cm^{-3} into account, the error due to viscosity is not significant enough to include in the uncertainty estimates. The data of Atilhan and Aparicio (2013) are represented within 0.075 % deviation by the equation of state.

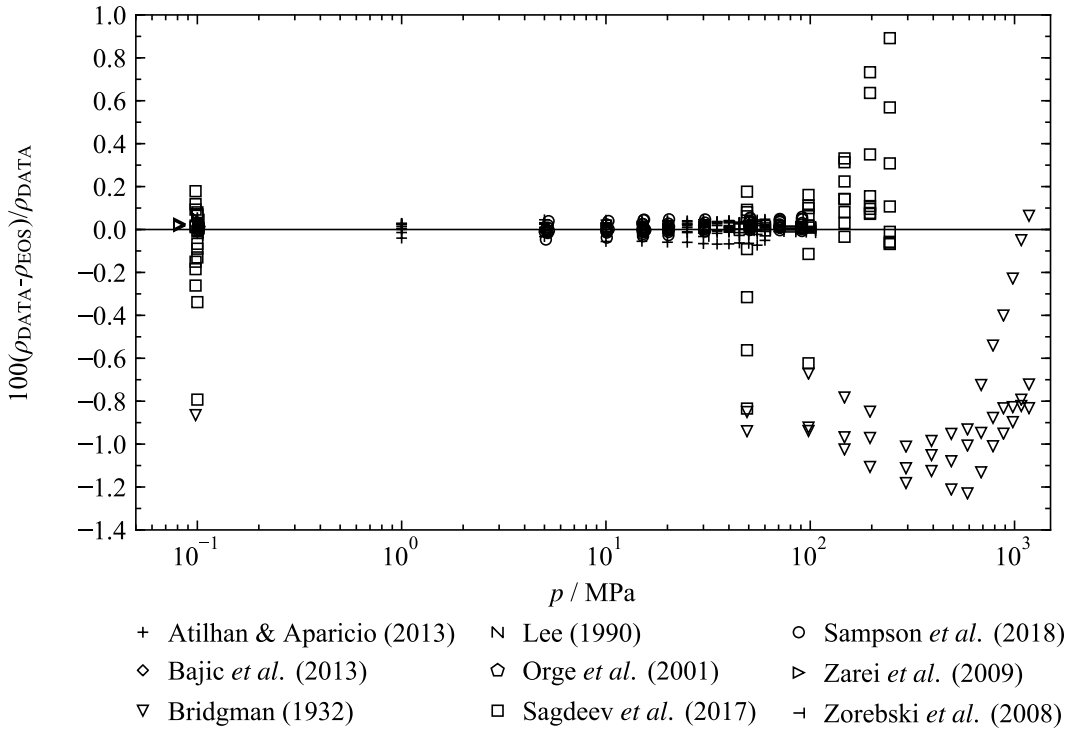

Figure 5.5 Deviations of single phase density data from the equation of state for selected data sets as a function of the logarithmic pressure.

The deviations of the investigated data sets are presented in Figure 5.5. Additionally, the mentioned data sets of Bridgman (1932) and Sadykov *et al.* (1974), which represent the data up to the pressure and temperature maximum of all underlying density measurements, are shown.

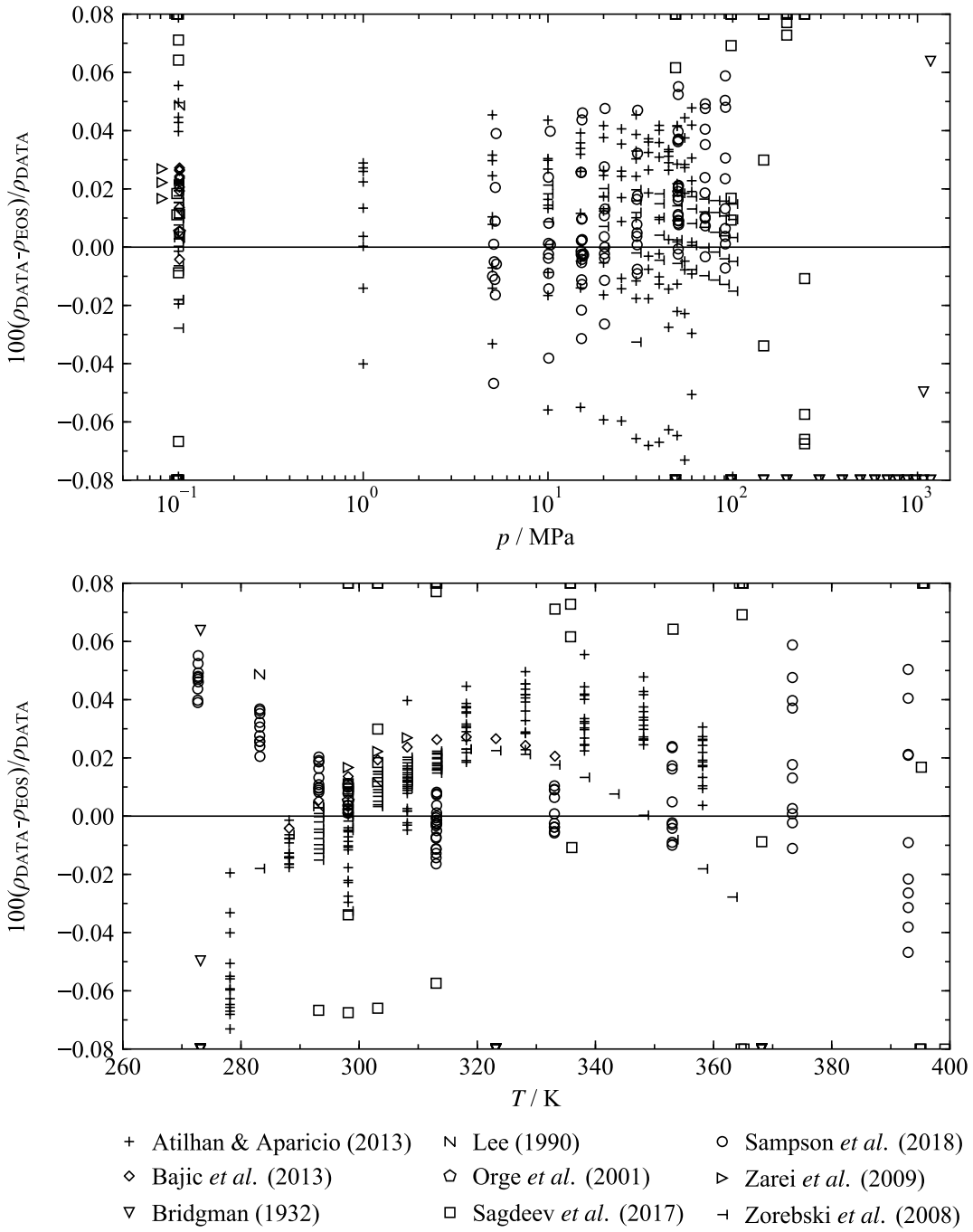

Figure 5.6 Deviations of selected single phase density data from the equation of state as a function of the logarithmic pressure (top) and the temperature (bottom).

In order to investigate the deviations of the fitted data sets of Sampson *et al.* (2018) and Atilhan and Aparicio (2013) as well as other corresponding data in more detail, Figure 5.6 shows temperature and pressure dependent plots for smaller deviation ranges.

A relatively large proportion of the single phase density data are covered by temperature dependent measurements at atmospheric pressure. Due to the limited temperature range, the area to be examined is fairly small. Figure 5.7 shows a larger number of data sets within 0.2 % of the equation. Except for the density measurement at atmospheric pressure obtained by Atilhan and Aparicio (2013), all selected data are not fitted to the equation of state.

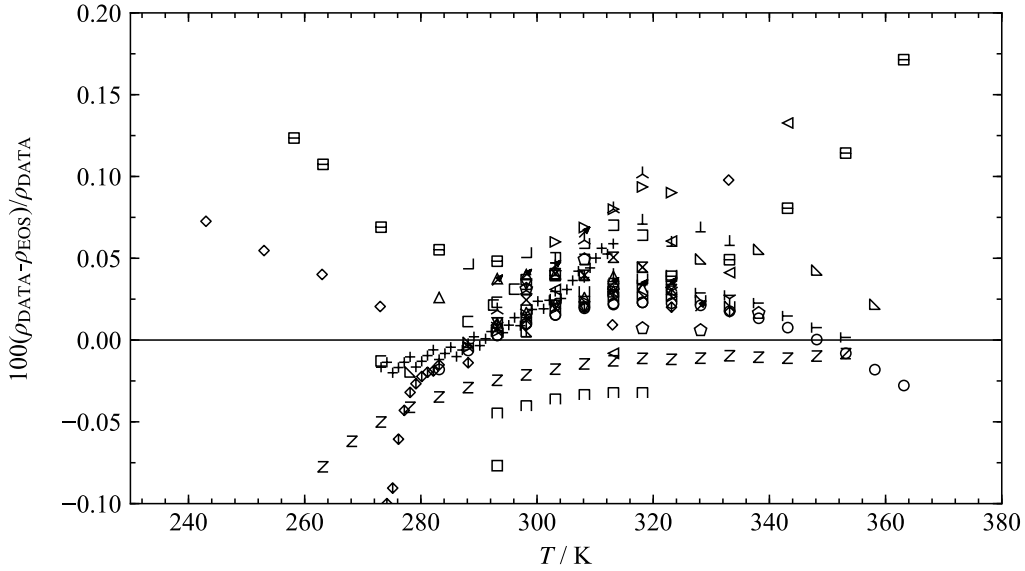

Atilhan & Aparicio (2013)
Bajic *et al.* (2013)
Curme *et al.* (1952)
Domanska *et al.* (2014)
Garber *et al.* (1970)
George & Sastry (2003)
Geyer *et al.* (2001)
Jimenez & Martinez (2006)
Li *et al.* (2007)
Li *et al.* (2008)
Ling *et al.* (2011)
Ling *et al.* (2016)
Makarov *et al.* (2016)
Marchetti *et al.* (2000)
Nain (2007)
Pal *et al.* (2016)
Ponedelnikova *et al.* (1954)
Saleh *et al.* (1999)
Soldatovic *et al.* (2016)
Srinivasa Krishna *et al.* (2015)
Timmermans & Hennaut-Roland (1955)
Tsai *et al.* (2009)
Vinogradov & Shakhparonov (1984)
Zarei *et al.* (2013)
Zemankova *et al.* (2013)
Zorebski *et al.* (2008)
Zvkovic *et al.* (2014)

Figure 5.7 Deviations of single phase density data from the equation of state for selected data sets at atmospheric pressure as a function of temperature.

5.7 Comparison of Vapor Pressure Data

The collected data sets, including 248 data points of vapor pressure measurements for propylene glycol, are presented in Table 5.6. The data cover a vapor pressure range from $2.7 \cdot 10^{-6}$ MPa to 0.27 MPa in a broad temperature range of 273 K to 493 K. Table 5.6 also shows the average absolute relative deviation of each data set.

Table 5.6 Summary of all underlying vapor pressure data along with the temperature and pressure ranges and their average absolute relative deviations (AAD) with respect to the equation of state.

Authors	Data points	T/K	p/MPa	AAD/%
Chyliński *et al.* (2004)	8	393 - 423	0.008 - 0.029	2.4
Clendenning *et al.* (1950)	1	459.15	0.101	4.8
Curme *et al.* (1952)	15	293 - 433	$1.1 \cdot 10^{-5}$ - 0.04	3.7
Dean (1999)	1	461.15	0.101	1.3
Fendu and Oprea (2014)	16	350 - 425	0.001 - 0.03	0.52
Gallant (1968)	1	460.45	0.101	0.84
Garcia and Paz Andrade (1974)	1	461.11	0.101	1.2
Gardner and Hussain (1972)	1	459.96	0.101	1.8
Giles *et al.* (1997)	2	373 - 453	0.003 - 0.081	1
Horstmann *et al.* (2001)	2	338 - 348	0.001	23.5
Hu *et al.* (2015)	1	460.70	0.101	0.042
Kundu *et al.* (1970)	9	278 - 318	$2.7 \cdot 10^{-6}$ - $8.9 \cdot 10^{-5}$	8.2
Mamedov *et al.* (2009)	1	461.15	0.101	1.3
Marcus (1998)	1	460.75	0.101	0.087
Marsden (1954)	10	319 - 461	$1.3 \cdot 10^{-4}$ - 0.101	6.3
Mathuni *et al.* (2011)	12	378 - 461	0.004 - 0.1	2.0
Musavirov *et al.* (1978)	1	460.11	0.101	1.9
Nageshwar and Mene (1968)	1	461.15	0.101	1.3
Puck and Wise (1946)	5	298 - 353	$1.8 \cdot 10^{-4}$ - 0.001	11.4
Rane *et al.* (2016)	17	389 - 443	0.007 - 0.06	4.2
Riddick and Toops, Jr. (1955)	7	298 - 461	$1.9 \cdot 10^{-4}$ - 0.10132	3.3
Riddick *et al.* (1986)	1	460.76	0.101	0.12
Schierholtz and Staples (1935)	1	460.55	0.101	0.53
Sevgili *et al.* (2008)	1	462.40	0.101	5.3
Shi *et al.* (1999)	1	460.76	0.101	0.12
Sokolov *et al.* (1971)	1	460.61	0.101	0.34
Sokolov *et al.* (1972)	5	356 - 461	0.001 - 0.101	3.0
Stull (1947)	10	319 - 461	$1.3 \cdot 10^{-4}$ - 0.101	6.3
Subramanian *et al.* (1978)	1	461.31	0.101	1.8
Verevkin (2004)	14	284 - 331	$4.3 \cdot 10^{-6}$ - $2.8 \cdot 10^{-4}$	5.7
Verevkin *et al.* (2009)	19	294 - 330	$1.2 \cdot 10^{-5}$ - $2.4 \cdot 10^{-4}$	3.9
Wilding *et al.* (1991)	4	348 - 473	0.001 - 0.081	3.21
Wilson *et al.* (1989)	2	273 - 313	$3.4 \cdot 10^{-6}$ - $9.1 \cdot 10^{-5}$	41.4
Xie and Chen (1993)	14	359 - 459	0.002 - 0.098	19.2

Authors	Data points	T/K	p/MPa	AAD/%
Yang *et al.* (2015)	1	460.69	0.101	0.073
Zhang *et al.* (2013)	21	390 - 461	0.007 - 0.1	1.3
Zhong *et al.* (2014)	1	460.22	0.101	1.5
Overall	245	273 - 461	$2.7 \cdot 10^{-6}$ - 0.101	

In the contemplation of all available vapor pressure data, it is mentionable that most of the measurements are limited to fairly small vapor pressures from roughly $3 \cdot 10^{-6}$ MPa to $5 \cdot 10^{-2}$ MPa. This has to be considered in assessing the percentage deviation of the data. Figure 5.8 gives an overview of all underlying vapor pressure data in a deviation range of 5 %.

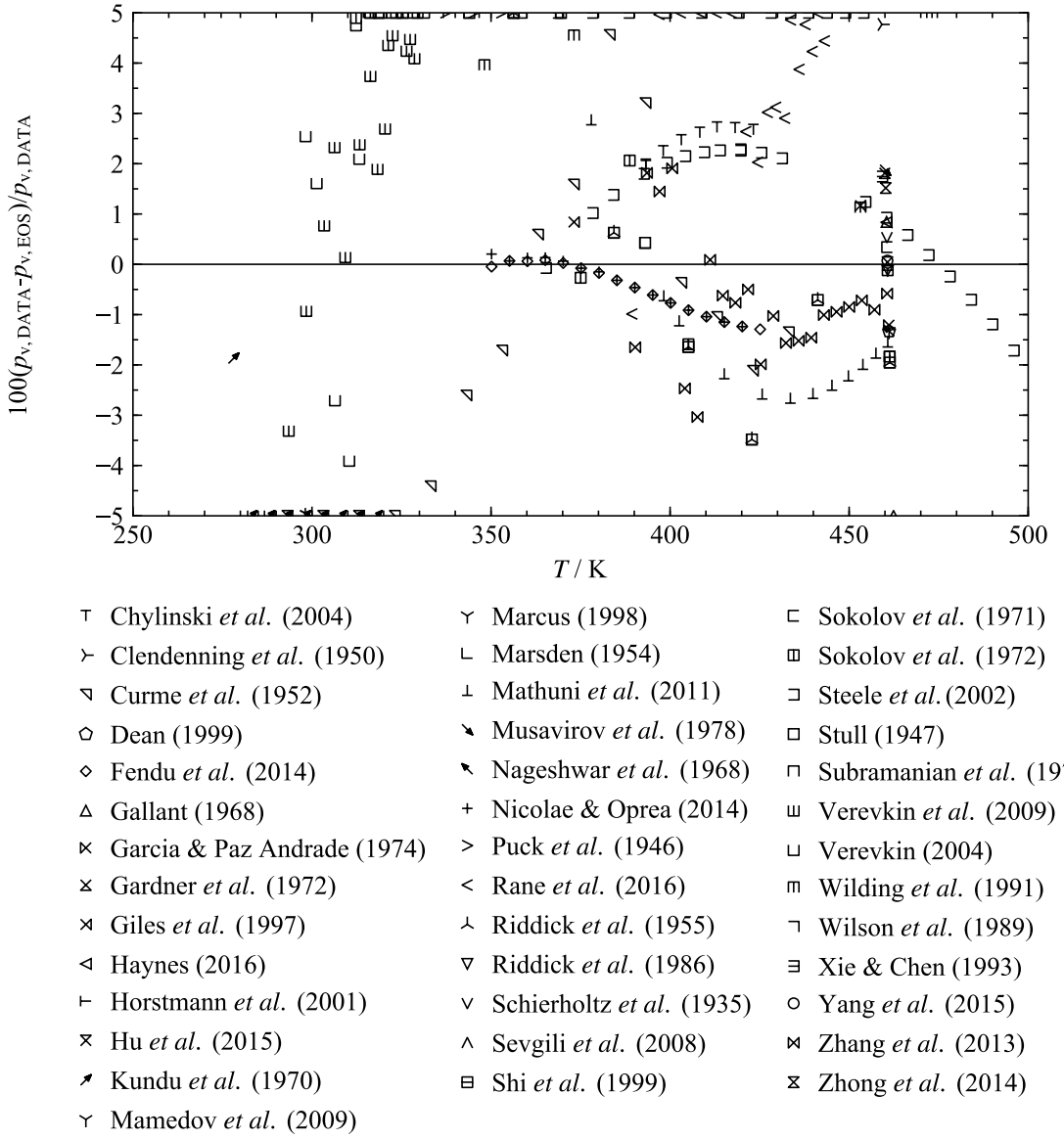

Figure 5.8 Deviations of all available vapor pressure data from the equation of state as a function of temperature.

Further, a few selected data sets are analysed in more detail. The representation of vapor pressure data by the equation of state can be shown by the two data sets of Nicolae and Oprea (2014) and Fendu and Oprea (2014), which provide vapor pressure measurements between 350 K and 420 K with reasonable uncertainties. In both publications the data were measured with the same apparatus in two independent series. The aim of the earlier publication by Nicolae and Oprea (2014) was to obtain reliable vapor-liquid equilibrium data for binary mixtures formed by dipropylene glycol and inferior aromatics. The mixture of propylene glycol and dipropylene glycol was only used for validating the experimental method by comparing obtained vapor pressures with the simulated results from the PRO/II 9.2 database. However, vapor pressure data for the pure propylene glycol were measured with the same apparatus as the actual measurements for the binary mixtures. Nicolae and Oprea (2014) used a static apparatus, consisting of an equilibrium cell, which is connected with a U-shaped tube and can be heated by a thermostatic oil bath. The U-shaped tube contains mercury, officiating as a manometric liquid. Further, a DPI 705 pressure sensor is attached to the tube in order to measure the sample' vapor pressure. Two assembled valves enable the communication with the atmosphere as well as with the vacuum pump. The two open ends of the U-shaped tube are connected by another valve, which only remains open during the degassing operation. Prior to the measurement, the sample was cooled close to the liquid nitrogen temperature and then degassed with the vacuum pump. The oil bath is used to heat up the equilibrium cell and the sample to its boiling temperatures at varying pressures. The bath is maintained at the desired temperature until the mercury level stays the same for at least 30 minutes, indicating a consistent pressure. This ensures that the equilibrium state is attained and that the temperature and pressure measurements can be considered as reasonable properties for the equilibrium state. The above described procedure is repeated a few times to keep the measurements as accurate as possible Nicolae and Oprea (2014). Fendu and Oprea (2014) measured vapor-liquid equilibrium data of propylene glycols systems and for the pure substances as well. In order to validate their experimental procedure, they refer to the data of Nicolae and Oprea (2014) obtained for pure propylene glycol, which are in very good agreement with the recent data of Fendu and Oprea (2014). With the exact same apparatus, a high consistency is also to be expected. For the given temperature range, both data sets contain corresponding vapor pressure data between 0.8 kPa and 25 kPa, roughly. According to this, the standard uncertainties are within 0.012 kPa and 0.034 kPa, which is equivalent to a range of percentage uncertainty of 0.14 % to 1.45 %. The two single point measurements of Hu *et al.* (2015) and Yang *et al.* (2015) yield well represented data at the normal

boiling temperature of 461 K. Prior to the determination of isobaric vapor-liquid equilibrium data for binary systems of carbonates and glycols, Hu *et al.* (2015) measured the boiling temperature at a pressure of 101.3 kPa for the pure compounds. The apparatus used is a dynamic recirculating still (Labodest VLE 602). The sample is heated with an immersion heater until the boiling temperature is reached. The two phase boiling sample then enters the Cottrell pump, which facilitates a close contact of the two phases and maintains vapor-liquid equilibrium. The pump leads the two phase sample into a phase separation chamber, from which the vapor phase is condensed by cooling water and recycled back. The disengaged liquid is well mixed with the condensed vapor before returning to the heater. After 30 minutes of stable temperature and pressure, the equilibrium state is considered to be attained and temperature and pressure are recorded with a Pt-100 and a digital manometer. The accuracies are claimed to be within a range of 0.1 K and 0.1 kPa (0.1 %). With a deviation of 0.04 %, the data point of Hu *et al.* (2015) is considered to be well represented by the equation. The other data point of Yang *et al.* (2015) is obtained from a similar Rose-Williams still apparatus. The temperature and pressure were measured with a mercury thermometer and a U-shaped differential manometer, which have uncertainties of 0.13 kPa and 0.01 K, respectively. With a uncertainty of 0.07 %, the data point is in very good agreement with the equation and consistent with the independent data point obtained by Hu *et al.* (2015). The vapor pressure data discussed above are shown in Figure 5.9.

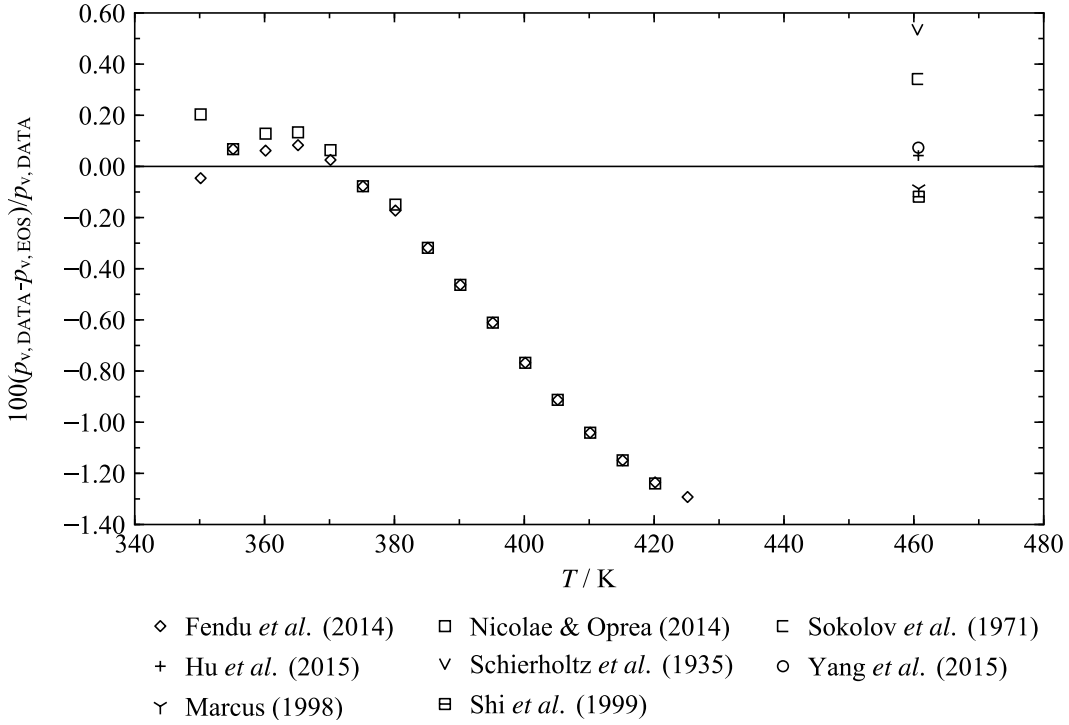

Figure 5.9 Deviations of the selected vapor pressure data from the equation of state as a function of temperature.

5.8 Comparison of Speed of Sound Data

The underlying data for speed of sound include 206 points from 14 publications and one personal communication. The data cover a temperature range of 258 K to 363 K and reach fairly high pressures up to 101 MPa. Table 5.7 gives an overview of all available data and their average absolute relative deviations (AAD) from the equation of state.

Table 5.7 Summary of all underlying speed of sound data along with the temperature and pressure ranges and their average absolute relative deviations (AAD) with respect to the equation of state.

Authors	Data points	T/K	p/MPa	AAD/%
Marks (1967)	3	273 - 353	0.101325	0.058
Kishimoto and Nomoto (1954)	6	288 - 313	0.101325	0.11
Grzybkowski and Warmińska (2016)	1	298.15	0.1	0.034
Zorebski *et al.* (2008)	45	293 - 313	0.1-101	0.027
Scholz (2017)	77	293 - 353	0.533-20	0.085
Tsierkezos and Palaiologou (2009)	1	298.15	0.101325	0.048
Krishna *et al.* (2015)	6	298 - 323	0.101325	0.16
Sastry and Patel (2003)	2	298 - 308	0.101325	1.5
Palani and Geetha (2009)	3	303 - 313	0.101325	0.24
Ponedelnikova and Tarasova (1954)	12	258 - 363	0.101325	0.26
Pal *et al.* (2016)	6	293 - 318	0.1	0.16
Nain (2008)	6	293 - 318	0.101325	0.55
George and Sastry (2003)	5	298 - 338	0.101325	0.89
Latha *et al.* (2015)	4	303 - 318	0.101325	0.14
Kushare *et al.* (2008)	1	298.15	0.101325	0.085
Dávila *et al.* (2016)	28	303 - 353	0.099 - 30.2	0.021
Overall	208	184 - 363	0.099 - 101	

Figure 5.10 gives an overview of the percentage deviations of all available speed of sound data in a range of 0.8 %. The data of Zorebski *et al.* (2008) contain speed of sound measurements in a temperature range of 292 K to 313 K from ambient pressure up to 101 MPa. With 45 data points, it represents a vast percentage of the data that cover a broad pressure range. The data of Zorebski are in very good agreement with the data set of Dávila *et al.* (2016), particularly for data at ambient pressure and temperatures between 303 K and 313 K.

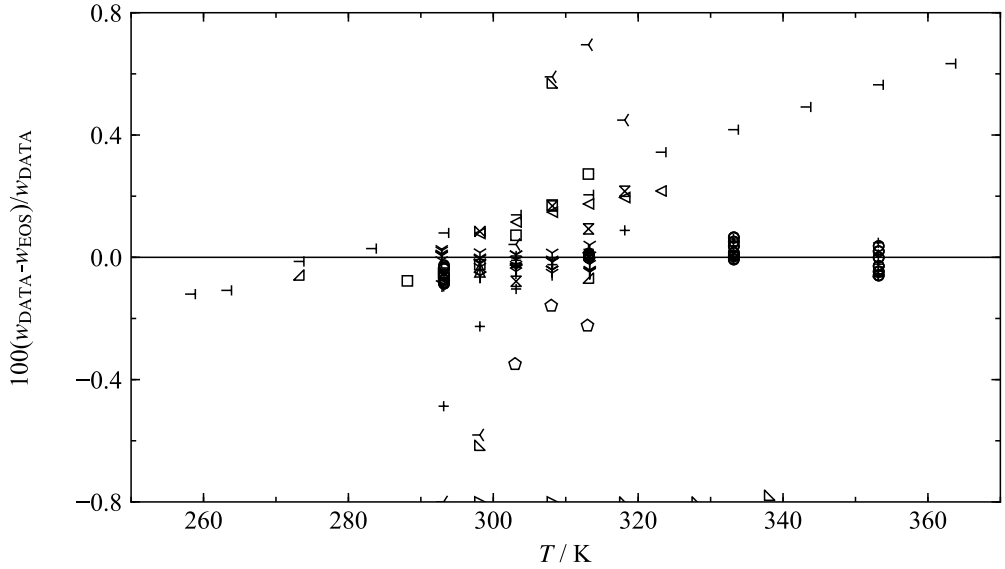

+ Davila *et al.* (2016)
◺ George and Sastry (2003)
∧ Grzybkowski and Warminska (2016)
□ Kishimoto and Nomoto (1954)
⋈ Kushare *et al.* (2008)
⧖ Latha *et al.* (2015)
◿ Marks (1967)
≺ Nain (2008)
+ Pal *et al.* (2016)
⬠ Palani and Geetha (2009)
⊣ Ponedelnikova *et al.* (1954)
▷ Sastry and Patel (2003)
○ Scholz (2018)
◁ Srinivasa Krishna *et al.* (2015)
△ Tsierkezos *et al.* (2009)
≻ Zorebski *et al.* (2008)

Figure 5.10 Deviations of all available speed of sound data from the equation of state as a function of temperature.

The measurements of Dávila *et al.* (2016), which consist of 28 data points, start at ambient pressure and go up to 30 MPa with a maximum temperature of 353 K. Zorebski *et al.* (2008) claim uncertainties of 1 m/s, which corresponds to a percentage deviation of 0.067 % over the examined temperature range. The uncertainty in the measurements of Dávila *et al.* (2016) is 0.02 %, partly because of the high purity of 99.87 %, as compared to the 99 % sample used by Zorebski *et al.* (2008). The uncertainty bands of the data points overlap and thus confirm the consistency of the data sets, assuming that uncertainties were estimated correctly. Both measurement were based on the ultrasonic pulse-echo-overlap method. The ultrasonic sensor is composed of a piezoelectric quartz crystal, which is aligned between two polished reflectors of unequal distances. The quartz crystal functioned as a transducer, sending and receiving ultrasonic signals and is electrically excited by two sinusoidal burst signals with a time difference Δt at its resonance frequency of 8 MHz Dávila *et al.* (2016). Zorebski *et al.* (2008) used a ceramic transducer with a resonance frequency of 2 MHz. The ultrasonic pulses, produced by the transducer, propagate in both directions, pass through the fluid, and are reflected at the ends of the cell. The time difference between the two signals and the amplitude of the second signal are adjusted so that the second echo of the first signal cancels the first echo of the second signal.

Thus, the time difference between the two excited signals is equal to the time difference between the two echoes and therefore gives the time difference Δt, which is used in the speed of sound calculation. The ultrasonic pulse-echo-overlap technique is predominantly used for measuring speed of sound in liquids and compressed gases at high pressure Gedanitz *et al.* (2010). In the pulse-echo-overlap method, the speed of sound of distinct wave phases is measured and the achievable accuracy can be relatively high Dzida *et al.* (2017).

Furthermore, the data set of Zorebski *et al.* (2008) is in very good agreement with two independent, single point measurements of Grzybkowski and Warmińska (2016) and Tsierkezos and Palaiologou (2009) at 298.15 K and atmospheric pressure. Grzybkowski and Warmińska (2016) claim an uncertainty of 0.15 m/s, which corresponds to a percentage deviation of 0.01 % for the data point. The data point was measured with the pulse-echo method, with a sample of 99.5 % purity. The measurement of Tsierkezos and Palaiologou (2009) has a similar purity, but has a higher uncertainty (1 m/s) and used a different measurement technique. Tsierkezos and Palaiologou (2009) obtained the speed of sound from an Anton Paar (DSA 48) sound analyser, which applies a modified sing-around technique. Contrary to the pulse-echo-overlap method, it operates with two single transducers, one for transmitting a short acoustic pulse into the sample and one for receiving it. After amplification, a signal re-excites the transmitter, which then sends another pulse. The measured repetition frequency of pulse transmissions contributes to the speed of sound estimation. Usually, this technique has high precision, but also requires complicated calibration procedures, which can cause considerable uncertainties Dzida *et al.* (2017).

Another measurement series was performed by Scholz (2017) in a pressure range between 0.5 MPa and 20 MPa at temperatures between 293.2 K and 353.2 K. The measurements are in very good agreement with the ones of Dávila *et al.* (2016), especially for pressures between 5 MPa and 20 MPa. At corresponding measurement temperatures (303 K, 333 K, and 353 K) the percentage deviations from the equation are less than 0.01 percentage points apart, which validates the high consistency of the two data sets. Both data sets lie within a deviation range of 0.087 % from the equation and are thus well represented. Scholz (2017) used a similar measurement technique based on the ultrasonic pulse-echo-overlap method as already described above. First analyses by Scholz (2017) yield uncertainties smaller than 0.08 % for measurements of a sample with 99.5 mol-% propylene glycol. The initial conservative assumptions are based on a 0.5 mol-% impurity with water. Figure 5.11 shows the pressure and temperature dependent deviations of the above investigated measurements in a range of 0.08%.

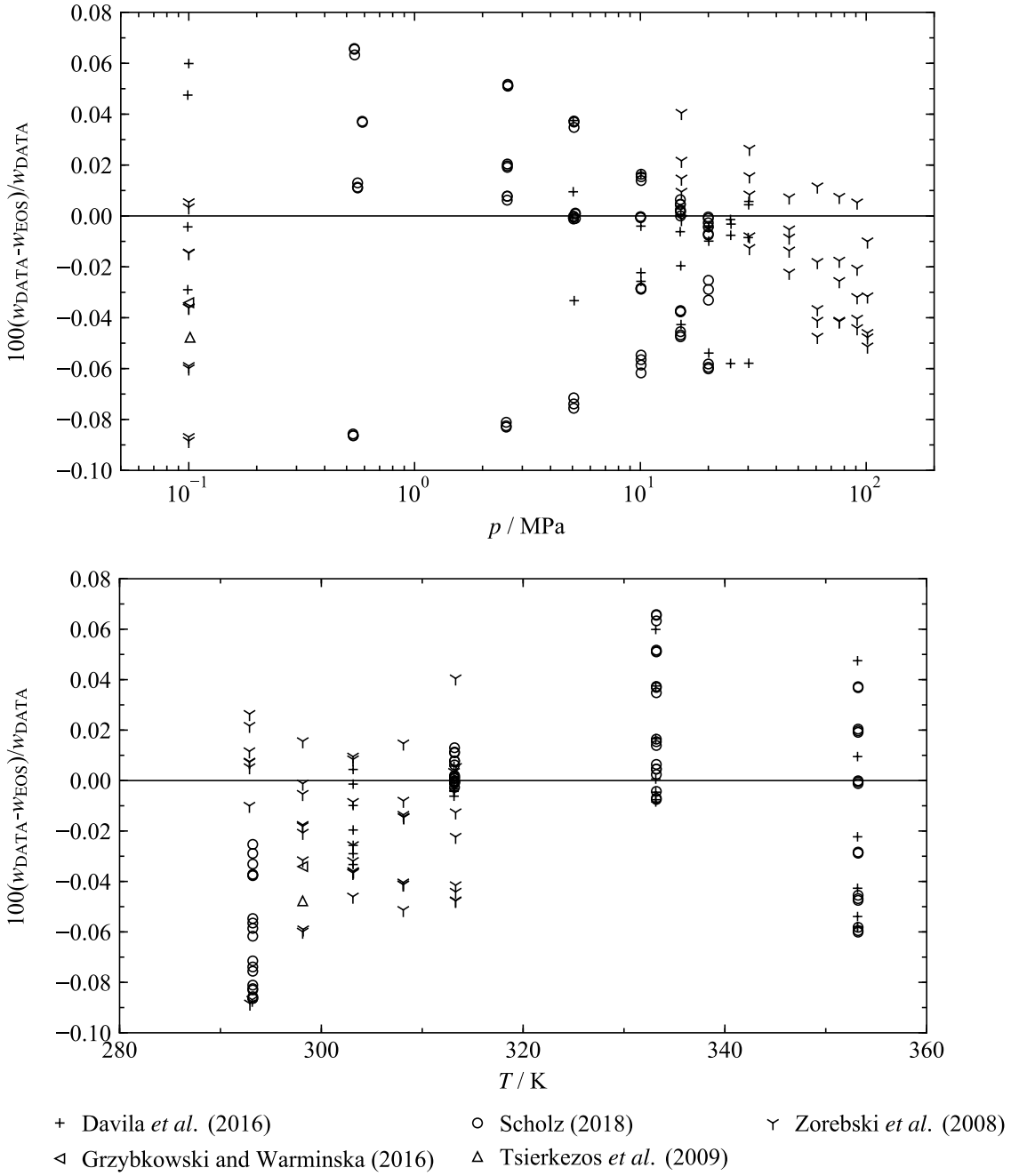

Figure 5.11 Deviations of selected speed of sound data from the equation of state as a function of the logarithmic pressure (top) and the temperature (bottom).

5.9 Comparison of Isobaric Heat Capacity Data

The underlying isobaric heat capacity data are obtained from four different sources with reasonable deviations from the equation. These data sets are listed in the first four lines of Table 5.8. All available data were measured at atmospheric pressure and temperatures between 283 K and 353 K.

Table 5.8 Summary of all underlying isobaric heat capacity data along with the temperature range and their average absolute relative deviations (AAD) with respect to the equation of state at atmospheric pressure

Authors	Data points	*T*/K	AAD (%)
Parks and Huffman (1927)	4	275-277	3.9
Dean (1999)	1	298.15	0.49
Riddick *et al.* (1986)	1	29315	0.90
Li *et al.* (2009)	6	303-353	0.40
Pietrzak and Łudzik (2015)	1	29815	0.01
Zemánková *et al.* (2013)	5	283-313	1.1
Overall	18	275-353	

The data set of Li *et al.* (2009) considers isobaric heat capacity data in a temperature range of 303 K and 353 K. The other sources consist of single data points, which yield measurements at temperatures of 293 K or 298 K. Li *et al.* (2009) used the differential scanning calorimeter (DSC) to measure the isobaric heat capacity of propylene glycol as well as several mixtures of glycols, water, and salts. More precisely, the DSC consists of a DSC-2010 cell and a thermal analysis controller. The temperature calibration is obtained from measurements of the melting point of indium. Li *et al.* (2009) claim uncertainties of 0.53 % to 0.6 %, which is equal to a deviation of 0.015 $kJ \cdot kg^{-1} \cdot K^{-1}$ for each measured data point. All data obtained by Li *et al.* (2009) are within 0.59 % deviation from the equation of state. The single data point by Pietrzak and Łudzik (2015) at 298 K is in a good agreement with the equation. In the measurements of the molar isobaric heat capacity of some pure 1,2-alkanediols, they use the differential scanning calorimeter Micro DSC III (Setaram). The data point of propylene glycol is measured with a claimed uncertainty of 0.15 % and is even more accurate with respect to the equation of state (0.014 %). The deviations of all available isobaric heat capacity data are shown in Figure 5.12.

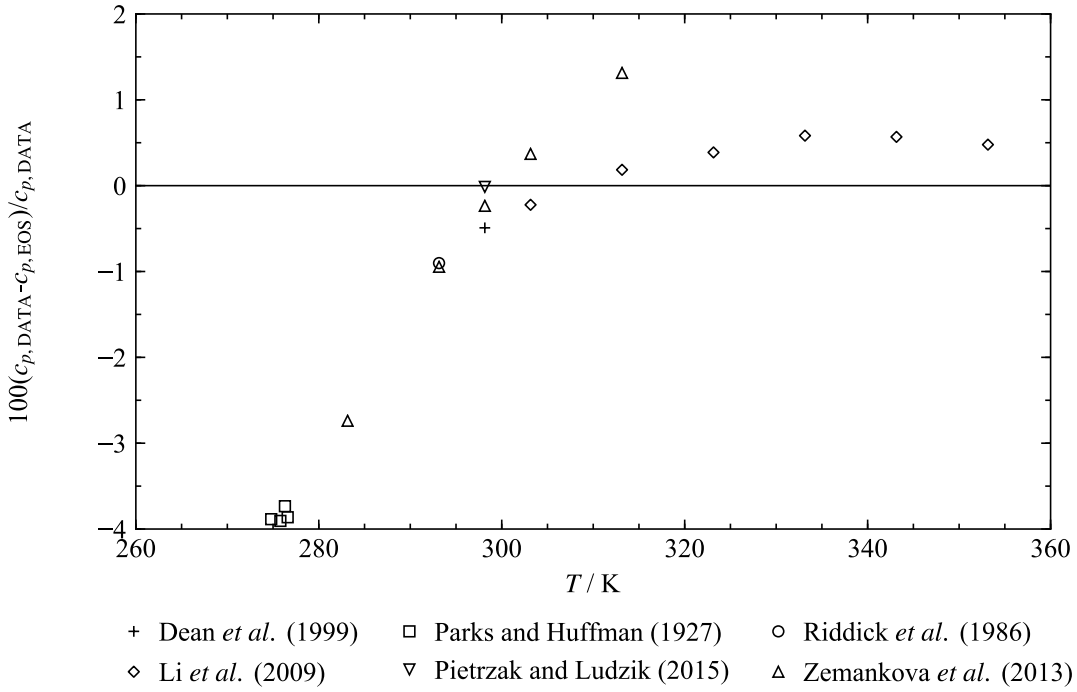

Figure 5.12 Deviations of all available isobaric heat capacity data from the equation of state as a function of temperature.

6 Extrapolation and Physical Behavior

In addition to the highly precise representation of the experimental data, the extrapolation behavior is also used to assess the quality of the equation of state. The constant property lines must have reasonable characteristics over the entire fluid state. To ensure the physically correct behavior of the equation in immoderate fluid state regions at either very high or low temperature and close to the critical point, a smooth and steady course of constant properties in those regions is very important. In this chapter, the behavior of various thermal and caloric properties of propylene glycol are investigated with respect to the criteria mentioned above and the compound specific effect of strong association.

The correct extrapolation behavior of thermal properties of propylene glycol is displayed in Figure 6.1. Isotherms and isobars converge for high values of pressure and density, without intersecting each other. The density behavior along isotherms and isobars should be smooth, steady, and free of any bumps, as is the case for propylene glycol. The values of isothermal density shown in Figure 6.1 go up to a temperature of 1000 K, while isobars are presented in a range of 1 MPa to 25 MPa.

To assess the representation of the fluid state close to the critical point, the critical isotherm in the p vs. ρ plot is evaluated closely with the use of the following two constraints at the critical temperature

$$\left(\frac{\partial p}{\partial \rho}\right)_T = 0 \tag{6.1}$$

and

$$\left(\frac{\partial^2 p}{\partial \rho^2}\right)_T = 0. \tag{6.2}$$

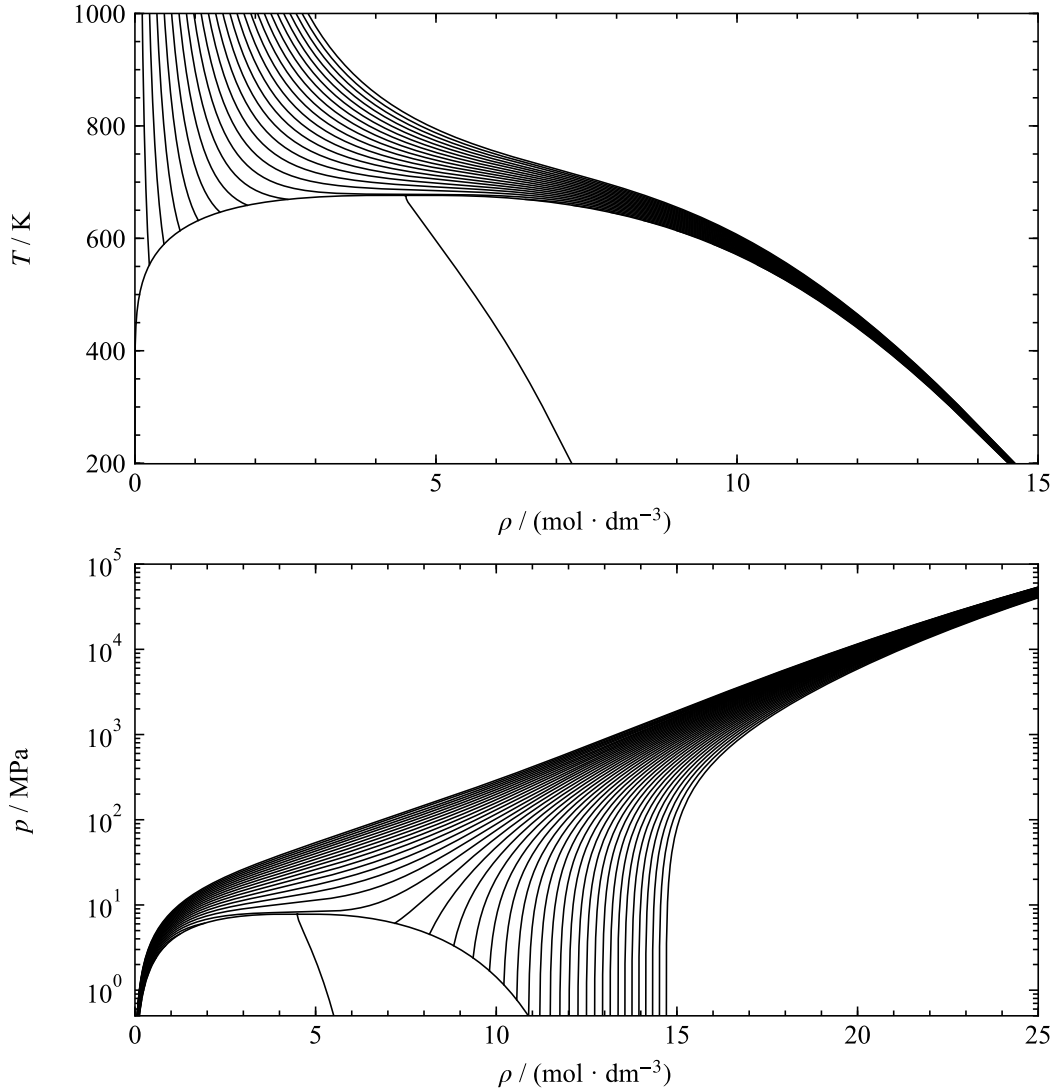

Figure 6.1 Behavior of the thermal properties of propylene glycol. Values are shown along isobars (top) and isotherms (bottom).

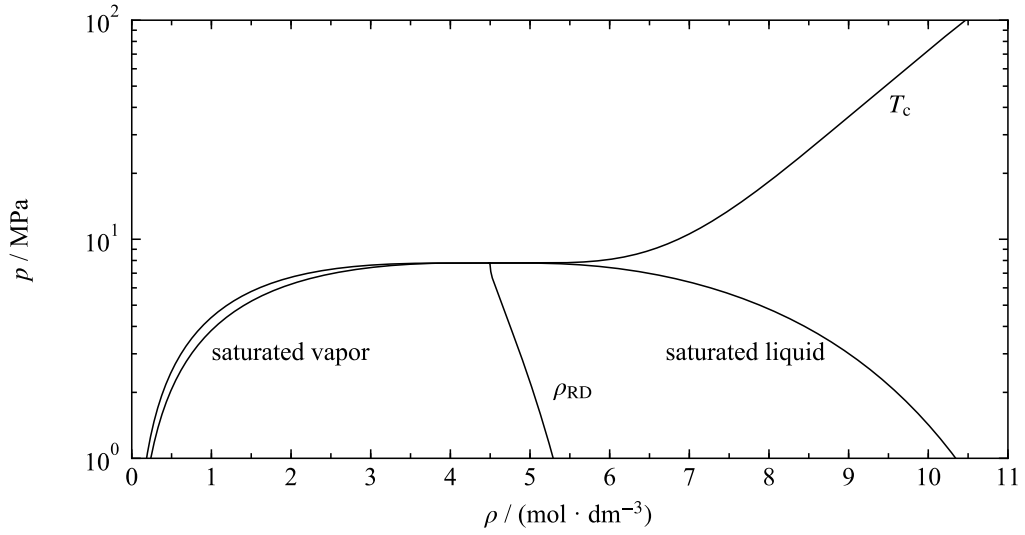

Figure 6.2 Density as a function of pressure including the critical isotherm (T_c) and the rectilinear diameter ($\rho_{RD} = 1/2\,(\rho' + \rho'')$).

Another quantity used to assess the quality of the equation of state in representing the critical region of fluids is the rectilinear diameter. The rectilinear diameter is the average of the densities and should be a linear function with respect to the density in the vicinity of the critical point. Starting in the two phase region, below the critical point, the rectilinear diameter is in good qualitative agreement with experimental data and ends exactly at the critical point according to Zollweg and Mulholland (1972). The course of the rectilinear diameter for propylene glycol in a p vs. ρ plot is presented in Figure 6.2.

The residual isochoric heat capacity of propylene glycol as a function of temperature is presented in Figure 6.3. The advantage of this plot is the ability to emphasize the characteristics of the liquid and vapor saturation lines, as well as the behavior at and near the critical point. Ideally, the saturation lines should cross once before they meet at the critical point, and should have a steep slope and positive curvature. Figure 6.3 shows only the real fluid behavior (i.e., the ideal gas contribution has been removed). According to this, the residual isochoric heat capacity needs to decay to its ideal gas limiting value of zero at high temperatures. This behavior is shown appropriately by the equation for propylene glycol.

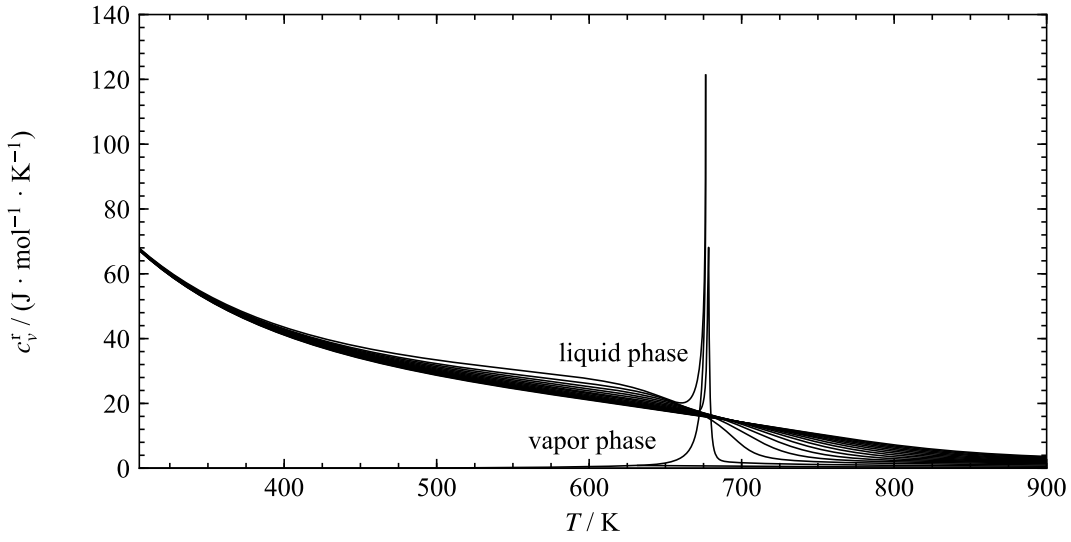

Figure 6.3 Residual isochoric heat capacity as a function of temperature.

The sound speed versus temperature is shown in Figure 6.4. The smooth isobars are shown, rising at lower temperatures. The equation is considered to behave appropriately within a broad temperature range and up to very high pressures. Below and close to the critical point, the first

two derivatives along saturation lines should be negative and the curvature of the vapor saturation line should be slightly stronger. At the critical point the two saturation lines reach their absolute minimum.

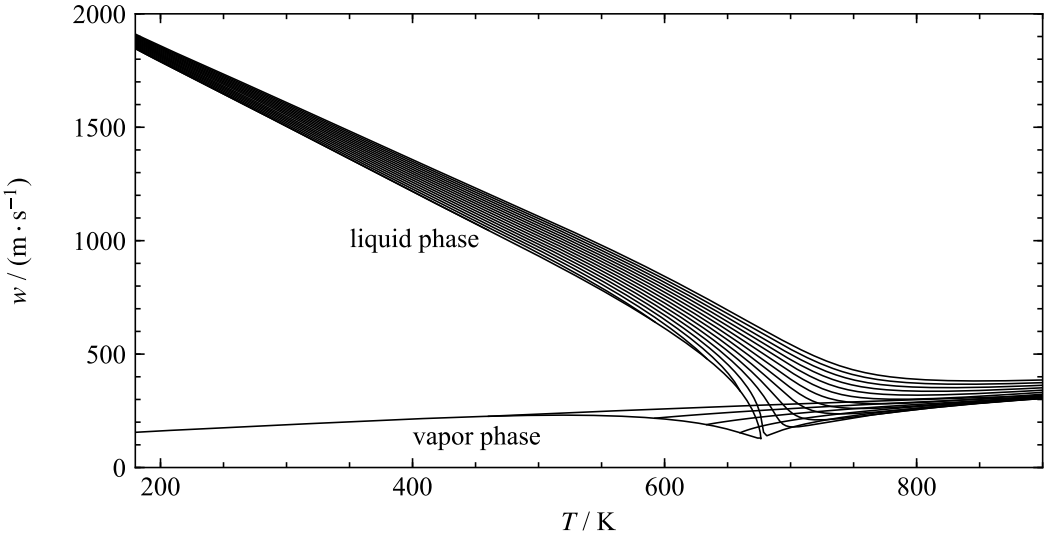

Figure 6.4 Speed of sound as a function of temperature along selected isobars.

The phase identification parameter (PIP) is an important property in examining the extrapolation behavior of the equation of state. Originally, the parameter was introduced by Venkatarathnam and Oellrich (2011) in order to differentiate vapor phase from liquid phase states. The PIP is defined as

$$\Pi = 2 - \rho \left[\frac{\partial^2 p/(\partial\rho\partial T)}{(\partial p/\partial T)_\rho} - \frac{(\partial^2 p/\partial\rho^2)_T}{(\partial p/\partial\rho)_T} \right]. \tag{6.3}$$

Through its high dependency on partial derivatives of pressure, volume, and temperature, the phase identification parameter is a significantly important property in considering the quality and the behavior of the equation. The values of the phase identification parameter in the liquid phase are greater than 1, and less than 1 in the vapor phase. Figure 6.5 displays the PIP versus temperature along isobars between 0.1 MPa and 30 MPa. The saturated liquid line has all positive derivatives starting from low temperatures to the critical point, where the PIP reaches very high values. The values along the saturated vapor line near the critical point decrease strongly with increasing temperature and reach an absolute minimum just before the critical point at the same temperature as the maximum for the saturated liquid state. The isobars need be smooth and change curvature at the critical point to ensure appropriate physical behavior in the critical region and also at very low or high temperatures.

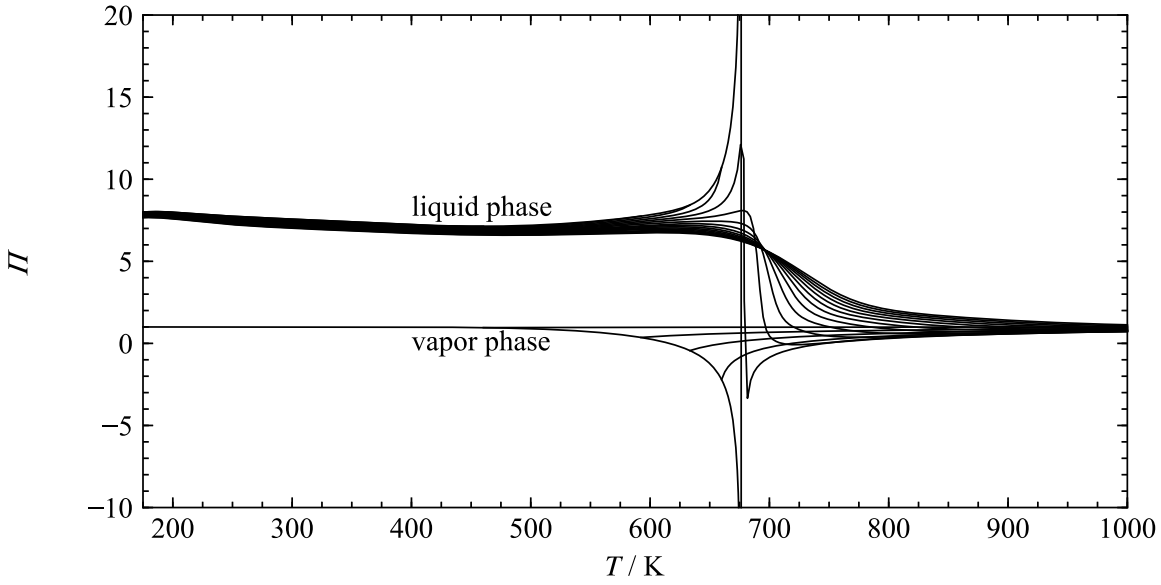

Figure 6.5 Phase identification parameter as a function of temperature along selected isobars.

The PIP versus density is presented in Figure 6.6 for temperatures between 170 K and 900 K. Isotherms at extremely high temperatures should cross at the critical point and at the same value of the PIP. Through the critical region, the curvature of isotherms should change, but in a very smooth way. For appropriate extrapolation behavior, the isotherms should ideally converge at higher densities.

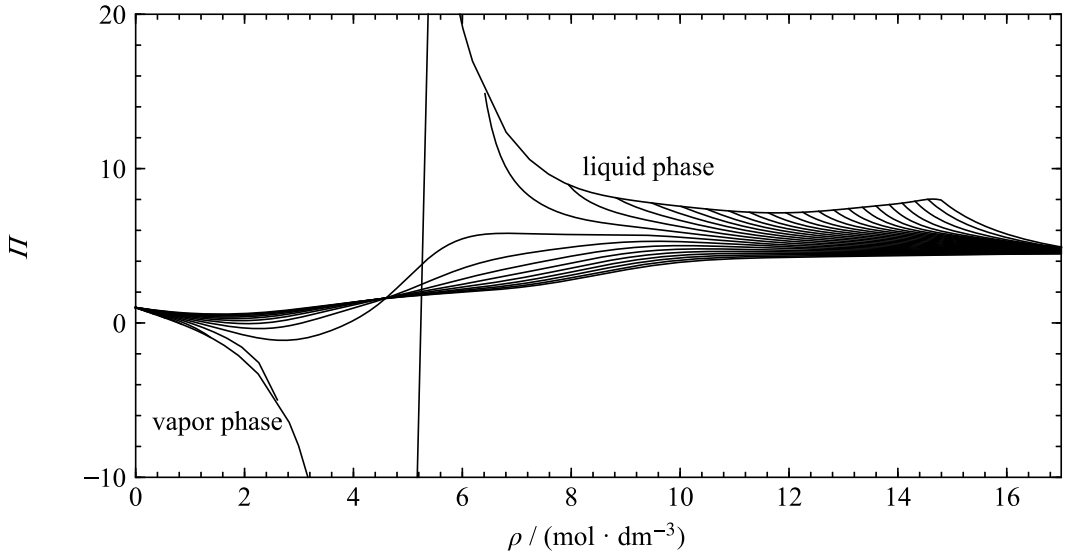

Figure 6.6 Phase identification parameter as a function of density along selected isotherms.

Another important parameter in investigating the quality and the extrapolation behavior of the equation of state is the Grüneisen parameter. It is defined as the ratio between the first pressure derivation with respect to the temperature and the isochoric heat capacity:

$$\Gamma = \frac{(\partial p/\partial T)_\rho}{\rho/c_v}. \tag{6.4}$$

The Grüneisen parameter has long been used in the approximation of the dependency of lattice frequencies on the change in volume of crystals. In 1970 it was extended from solid to liquid states and was then used as a fairly sensitive parameter in validating the behavior of equations of state Arp *et al.* (1984). The Grüneisen parameter is directly related to the isochoric heat capacity and thus some characteristics of the Grüneisen parameter versus temperature are comparable with the speed of sound behavior. The most visible difference is seen in the behavior of the boiling line, which inclines to smaller values for lower temperatures for this equation of state. As for the speed of sound, the two saturation lines should meet at the critical point and should be at their absolute minimum, which is shown in Figure 6.7. The smooth course of the isobars indicates reasonable behavior up to higher pressures and temperatures.

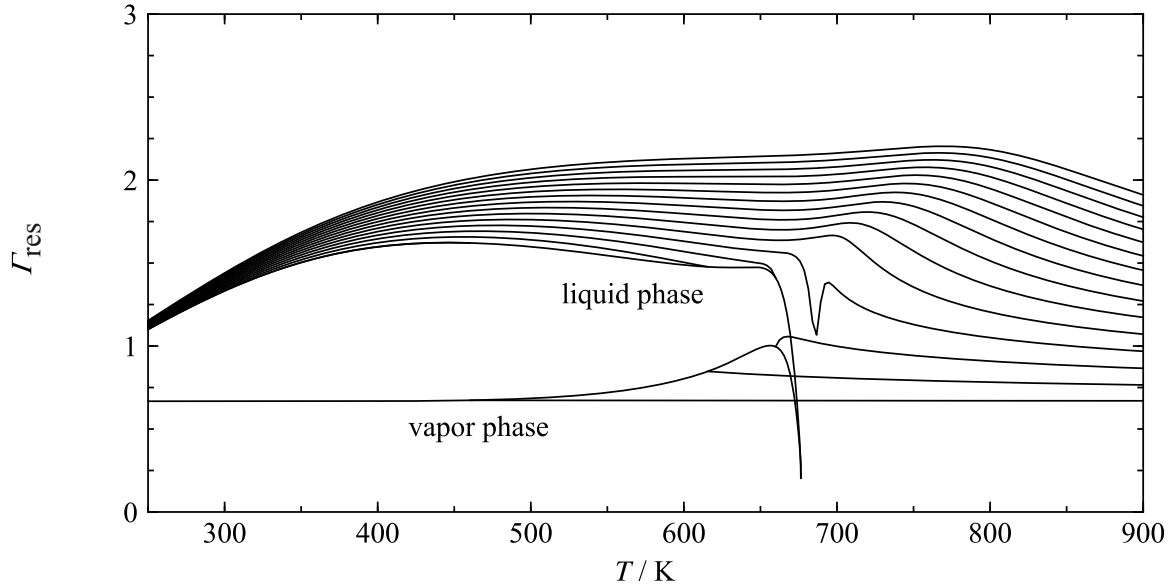

Figure 6.7 Residual Grüneisen parameter as a function of temperature along selected isobars .

Figure 6.8 displays the Grüneisen parameter as a function of density. The smooth and steady course of the isotherms demonstrate the appropriate behavior of the equation.

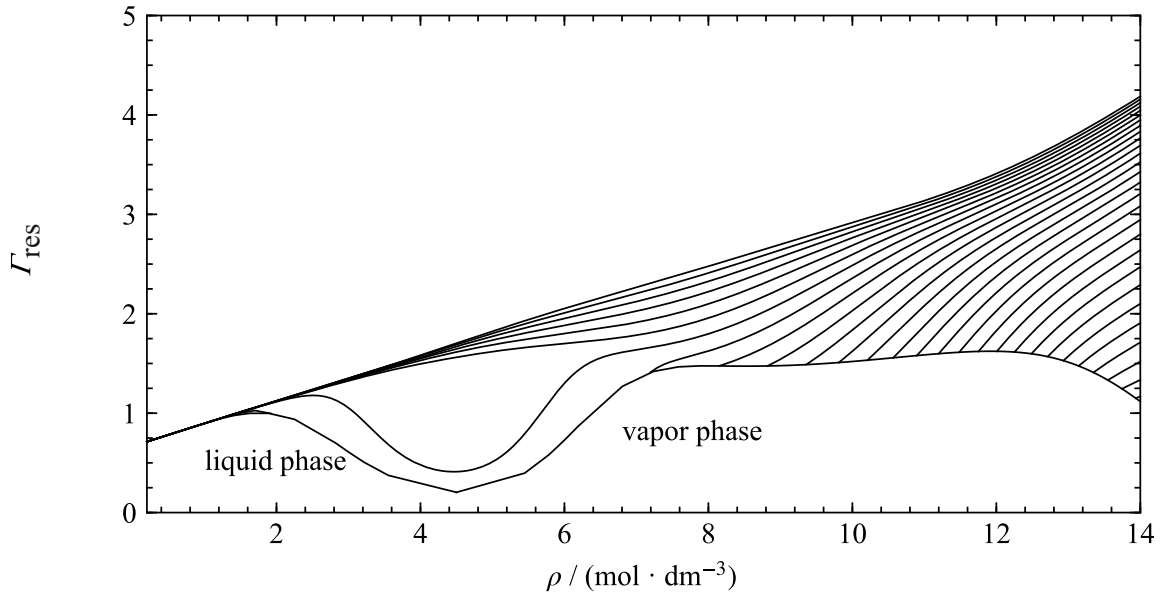

Figure 6.8 Residual Grüneisen parameter as a function of density along selected isotherms.

In Figure 6.9 the characteristic ideal curves of the equation of state is displayed as a function of reduced temperature T/T_c and pressure p/p_c. The ideal curves are an important property to assess the extrapolation behavior of the equation in regions without available data, which are usually up to temperatures and pressure above the critical point. This is further explained in section 4. The ideal curves are defined in terms of the compressibility factor Z and include the Boyle curve, the Joule-Thomson inversion curve, the Joule inversion curve, and the ideal curve. Since the properties of the real fluid are equal to the hypothetical ideal gas along the ideal curves for equal temperature and density, they can be defined in terms of the first derivative of the compressibility factor with respect to temperature and density as given in Table 6.1.

Table 6.1 Definition of the ideal curves in terms of the compressibility factor.

Expression	Compressibility factor	
Ideal curve	$Z = \frac{p}{\rho RT} = 1$	(5.8)
Boyle curve	$\left(\frac{\partial Z}{\partial \rho}\right)_T = 0$	(5.9)
Joule-Thomson inversion curve	$\left(\frac{\partial Z}{\partial T}\right)_p = 0$	(5.10)
Joule inversion curve	$\left(\frac{\partial Z}{\partial T}\right)_\rho = 0$	(5.11)

The reasonable extrapolation behavior of the equation is verified by the smooth course of the ideal curves as shown in Figure 6.9.

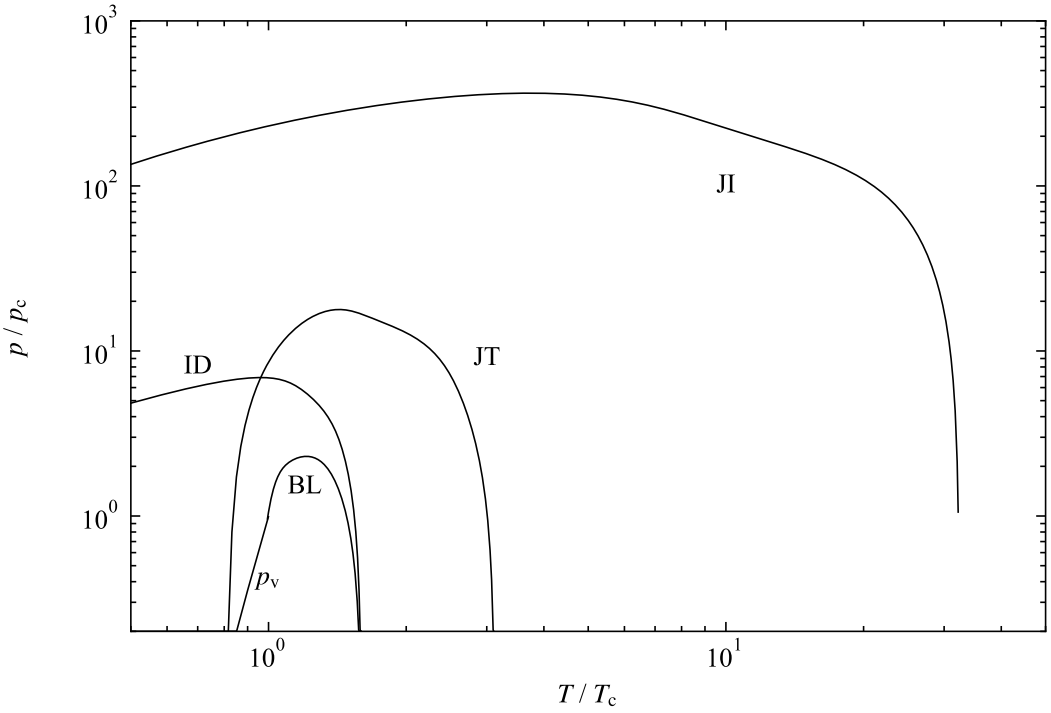

Figure 6.9 Ideal curves for the equation of state for propylene glycol in terms of reduced temperature T/T_c and pressure p/p_c: Vapor pressure curve (p_v), Boyle curve (BL), Joule-Thomson inversion curve (JT), Joule inversion curve (JI), and the ideal curve (ID).

Although the characteristic ideal curves of the equation of state show a generally appropriate behavior, it is mentionable that the Joule-Thomson inversion curve and the Joule inversion curve differ slightly from the desired course at reduced temperatures of T/T_c = 2 and T/T_c 10, respectively, so that the curvatures show a flattened shape.

A last considered criteria for assessing the extrapolation behavior of the equation are the virial coefficients. The virial coefficients can be obtained from experimental $p\rho T$ or speed of sound data and are often considered as a second source for thermal properties in the gas phase or supercritical gas like states according to Span (2000). Due to the fact that the virial coefficients are directly related to experimental data, uncertainties could be considered as a reasonable criteria for evaluating the extrapolation behavior of the equation. Predominantly, the overall behavior and shape of virial coefficients are used as a criterion to assess the extrapolation behavior, rather than uncertainties, which are relatively difficult to assign. The behavior of the second and third virial coefficients should be similar to each other, with C having a sharper form than B. Both go to negative infinity in the limit of zero temperature and cross the zero line at moderate temperatures. Each of them show a maximum at different temperatures and approach zero at extremely high temperatures. The theoretical behavior of the fourth virial coefficient D is defined by a second maximum at higher temperatures than the first, though the magnitude of

the second maximum is fairly smaller according to Thol (2015). The overall behavior of the virial coefficients is shown in Figure 6.10. Whereas the second and third virial coefficients show an appropriate course, the fourth coefficient lacks in presenting the global maximum at smaller temperatures.

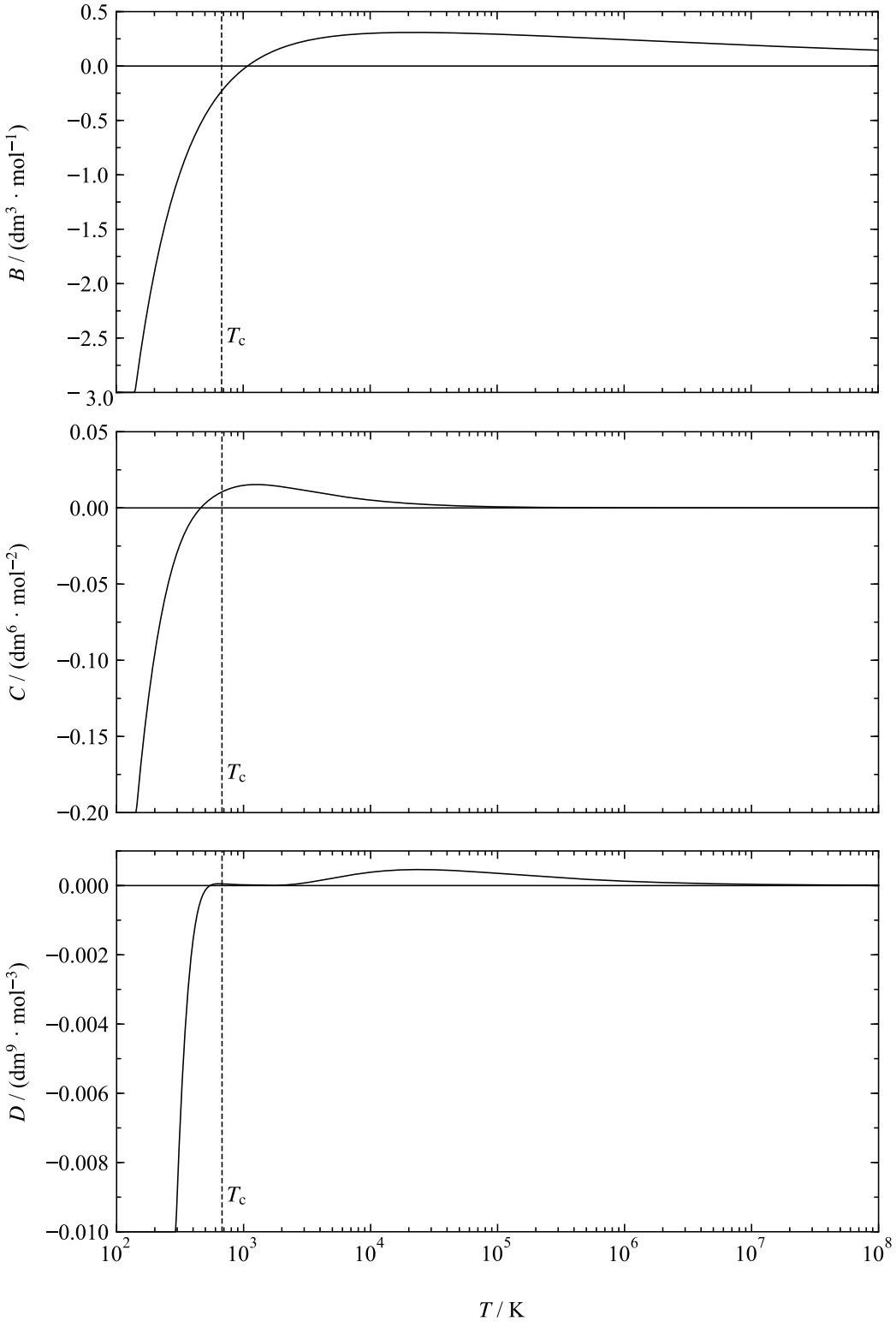

Figure 6.10 Second (B), third (C), and fourth (D) virial coefficient as a function of temperature.

7 Conclusion

The aim of this work was to develop a fundamental equation of state for propylene glycol in terms of the Helmholtz energy, consisting of an ideal and a residual part. The ideal part includes three Planck-Einstein terms, while the residual part has seven exponential, seven polynomial, and six Gaussian bell shaped terms. Ancillary equations for saturated densities and vapor pressure have been developed and can be used for fast approximate calculations of saturation properties as well as for initial estimates for the iterative calculation of properties at vapor-liquid equilibrium.

The range of validity covers states from the triple point temperature T_{tr} = 214 K to a maximum temperature of T_{max} = 450 K and a maximum pressure of p_{max} = 245 MPa. The equation can reliably be extrapolated to higher pressures up to 1200 MPa. Due to the limited temperature and pressure ranges of the available property measurements, the equation is expected to be less accurate for states not covered by data and are only extrapolations of the equation of state. This is problematic for single phase densities above areas where measurements are not available, in particular above 450 K. Due to thermal decomposition of propylene glycol at higher temperatures a broad temperature range from 450 K up to the critical temperature T_{c} = 676.4 K is not covered by data. In addition to the lack of data, the critical density was fitted simultaneously while fitting the other parameters. It was challenging to obtain an appropriate shape for the rectilinear diameter close to the critical point since its linear behavior is determined by the average of the liquid and vapor phase densities, which are not available for this fluid.

Considering all fitted density data in the liquid phase and at atmospheric pressure, the calculation uncertainty is 0.06 % in a temperature range from 278 K to 363 K. For higher pressures up to 90 MPa, the uncertainty increases up to 0.08 % between 272 K and 288 K. For comparable pressure ranges and for temperatures of 288 K to 328 K the calculated liquid phase density uncertainty is 0.04 %. To higher temperatures at 393 K, the equation becomes less accurate in representing the liquid phase densities (0.06 %). The available data for vapor pressures only cover a temperature range up to the normal boiling point at 461 K. The uncertainties in the normal boiling point data of the equation is less than 0.075 %. The equation is significantly less accurate in the temperature range from 350 K to 430 K, with an uncertainty up to 1.4 %. The speed of sound data are overall well represented by the equation of state for temperatures be-

tween 293 K and 353 K and pressures up to 100 MPa, with an uncertainty of 0.1 %. The calculation uncertainty for the isobaric heat capacity is determined by the available measurements in a temperature range from 300 K to 353 K at atmospheric pressure and is expected to be smaller than 0.6 %. Due to the lack of measurements for the ideal-gas isobaric heat capacity, it was difficult to corroborate the appropriate behavior of the ideal part of the equation of state. During the fitting process, initial assumptions were taken from the equation of state for ethylene glycol, since the two fluids are known to have similar physical behavior. Furthermore, the unmodified group contribution method for estimating ideal-gas isobaric heat capacities by Joback is presumed to be unsuitable for associating fluids, with the equation of state showing large uncertainties with respect to those predictions. The equation still shows large uncertainties, considering a modified equation for the ideal-gas isobaric heat capacity. This suggests the assumption that the equation of state may need to be improved in regard to the ideal behavior.

Plots of the thermal and caloric properties calculated with the equation of state shows a reasonable extrapolation behavior. The equation can appropriately be extrapolated to very high temperatures and pressures and low temperatures. A few notable effects with respect to the shape of the thermal and caloric property plots are likely to be related to the associating behavior of propylene glycol. For instance, the slope of isobars in the Grüneisen vs. temperature plot is negative at low temperatures. This effect can also be observed for ethylene glycol, which is considered to have similar association behavior. Furthermore, the virial coefficients follow appropriate behavior, except for the fourth.

The developed equation of state for propylene glycol is a suitable first approach to calculate properties with reasonable accuracy in a limited range of temperature and pressure. In the future, the equation of state will be further examined taking the extension of accessible data areas and the improvement of accuracy close to the critical point into account.

8 References

P. Ahlström; G. Wahnström; P. Carlsson; S. Schantz; A. Brodin; F. Maurer; L. Torell (1998): *Low-Frequency Vibrations in Monomers, Dimers and Polymers of Propylene Glycol*, Philosophical Magazine B **2**:699–707.

S. P. Andersson; O. Andersson (1998): *Relaxation Studies of Poly(Propylene Glycol) Under High Pressure*, Macromolecules 2999–3006.

C. A. Angell (1995): *Formation of Glasses from Liquids and Biopolymers*, American Association of Adv. Science **5206**:1924–1935.

V. Arp; J. M. Persichetti; G. Chen (1984): *The Grüneisen Parameter in Fluids*, J. Fluids. Eng. **2**:193–200.

M. Atilhan; S. Aparicio (2013): *PρT Measurements and Derived Properties of Liquid 1,2-Alkanediols*, J. Chem. Thermodyn. 137–144.

A. G. Badalyan; A. S. Keramidi; D. S. Kurumov (1989): *The density of normal octane in a wide range of state parameter*, Viniti, Code 3008-89:1–25.

D. M. Bajić; G. R. Ivaniš; Z. P. Visak; E. M. Zivković; S. P. Šerbanović; M. L. Kijevčanin (2013): *Densities, Viscosities, and Refractive Indices of the Binary Systems (PEG200+1,2-Propanediol, +1,3-Propanediol) and (PEG400+1,2-Propanediol, +1,3-Propanediol) at (288.15 to 333.15)K and Atmospheric Pressure*, J. Chem. Thermodyn. 510–529.

M. Benedict; G. B. Webb; L. C. Rubin (1940): *An Empirical Equation for Thermodynamic Properties of Light Hydrocarbons and Their Mixtures I. Methane, Ethane, Propane And n-Butane*, J. Chem. Phys. 334–345.

P. Boutron; A. Kaufmann (1979): *Stability of The Amorphous State in The System Water - 1,2-Propanediol*, Cryobiology 557–568.

P. W. Bridgman (1932): *Volume-Temperature-Pressure Relations for Several Non-Volatile Liquids*, Proc. Am. Acad. Arts Sci. **1**:1–27.

K. Chyliński; Z. Fraś; S. K. Malanowski (2004): *Vapor−Liquid Equilibrium for Propylene Glycol + 2-(2-Hexyloxyethoxy)ethanol and 1-Methyl-2-pyrrolidone + 1-Methoxypropan-2-ol*, J. Chem. Eng. Data **1**:18–23.

É. Clapeyron (1834): *Mémoire sur la puissance motrice de la chaleur*, Journal de l'Ecole Polytechnique 153–190.

K. A. Clendenning; F. J. MacDonald; D. E. Wright (1950): *Effects of Position Isomerism on the Physical Properties of Glycols*, Can. J. Res. Sec. B 608–622.

R. D. Cox (2004): *Ethylen Glycol Toxicity*, Military Medicine **8**:660–663.

G.O.,Jr. Curme; W.S. Jones; W.S. Tamplin (1952): *Glycols - Chapter 9: Physical Properties of Propylene Glycol*, Am. Chem. Soc. Mon. Ser. 210–240.

M. J. Dávila; H. Gedanitz; R. Span (2016): *Speed of Sound in Saturated Aliphatic Alcohols (Propan-2-ol, Butan-2-ol, and 2-Methylpropan-1-ol) and Alkanediols (Ethane-1,2-Diol, Propane-1,2- and -1,3-Diol) at Temperature between 253.15 K and 353.15 K and Pressures up to 30 MPa*, J. Chem. Thermodyn. 199–206.

J. A. Dean (1999): *Lange's Handbook of Chemistry*, McGraw-Hill.

P. G. Debenedetti; F. H. Stillinger (2001): *Supercooled Liquids and the Glass Transition*, Macmillan Magazines Ltd 259–267.

E. Diaz; M. E. Sad; E. Iglesia (2010): *Homogeneous Oxidation Reactions of Propanediols at Low Temperatures*, ChemSusChem 1063–1070.

V. Diky; R. D. Chirico; C. D. Muzny; A. F. Kazakov; K. Kroenlein; J. W. Magee; I. Abdulagatov; M. Frenkel (2013): *ThermoData Engine (TDE): Software Implementation of the Dynamic Data Evaluation Concept. 9. Extensible Thermodynamic Constraints for Pure Compounds and New Model Developments*, Am. Chem. Soc. 3418–3430.

U. Domańska; P. Papis; J. Szydłowski; M. Królikowska; M. Królikowski (2014): *Excess Enthalpies of Mixing, Effect of Temperature and Composition on the Density, and Viscosity and Thermodynamic Properties of Binary Systems of {Ammonium-Based Ionic Liquid + Alkanediol}*, J. Phys. Chem. B **44**:12692–12705.

M. Dzida; E. Zorebski; M. Zorebski; M. Zarska; M. Geppert-Rybczynska; M. Chorazewski; I. Cibulka (2017): *Speed of Sound and Ultrasound Absorption in Ionic Liquids*, Chemical Reviews **5:**3883–3929.

E. M. Fendu; F. Oprea (2014): *Vapor–Liquid Equilibrium for Propylene Glycols Binary Systems*, Fluid Phase Equilib. 244–253.

R. W. Gallant (1968): *Physical Properties of Hydrocarbons. 14. Propylene Glycols and Glycerine*, Gulf Publishing Company.

Yu.N. Garber; L.F. Komarova; L.I. Aleinikova; L.S. Fomina (1970): *Rectification of the Products Formed by Interaction of Propylene Oxide with Ethyl and Propyl Alcohols*, Zh. Prikl. Khim. 2658–2665.

M. Garcia; M. I. Paz Andrade (1974): *Funciones Termodinamicas De Exceso A 25°CI. Mezclas Diol + n-Alcohol*, Anal. De quim **70**:489–495.

P. J. Gardner; K. S. Hussain (1972): *The Standard Enthalpies of Formation of some Aliphatic Diols*, J. Chem. Thermodyn. **6**:819–827.

H. Gedanitz; M. J. Dávila; E. Baumhögger; R. Span (2010): *An Apparatus for the Determination of Speeds of Sound in Fluids*, J. Chem. Thermodyn. 478–483.

J. George; N. V. Sastry (2003): *Densities, Dynamic Viscosities, Speeds of Sound, and Relative Permittivities for Water + Alkanediols (Propane-1,2- and -1,3-diol and Butane-1,2-, -1,3-, -1,4-, and -2,3-Diol) at Different Temperatures*, J. Chem. Eng. Data **6**:1529–1539.

H. Geyer; P. Ulbig; M. Görnert (2000): *Measurement of Densities and Excess Molar Volumes for (1,2-Ethanediol, or 1,2-Propanediol, or 1,2-Butanediol+ Water) at the Temperatures (278.15, 288.15, 298.15, 308.15, and 318.15) K and for (2,3-Butanediol + Water) at the Temperatures (308.15, 313.15, and 318.15) K*, J. Chem. Thermodyn. **12**:1585–1596.

H. Geyer; P. Ulbig; M. Görnert; A. Susanto (2001): *Measurement of Densities and Excess Molar Volumes for (1,2-Propanediol, or 1,2-Butanediol+ Water) at the Temperatures (288.15, 298.15, and 308.15) K and at the Pressures (0.1, 20, 40, and 60) MPa*, J. Chem. Thermodyn. **9**:987–997.

N. F. Giles; L. C. Wilson; G. M. Wilson; W. V. Wilding (1997): *Phase Equilibria on Eight Binary Mixtures*, J. Chem. Eng. Data **6**:1067–1074.

W. Grzybkowski; D. Warmińska (2016): *Apparent Molar Volumes and Isentropic Compressibilities of Tetraalkylammonium Bromides in Aqueous Propane-1,2-diol. An Attempt to Design Hydraulic Liquids*, J. Chem. Eng. Data **9**:2933–2945.

B. Guignon; C. Aparicio; P. D. Sanz (2010): *Volumetric Properties of Pressure-Transmitting Fluids up to 350 MPa - Water, Ethanol, Ethylene Glycol, Propylene Glycol, Castor Oil, Silicon Oil, and Some of Their Binary Mixture*, J. Chem. Eng. Data **9**:3017–3023.

L. Haar; J. S. Gallagher; G. S. Kell (1982): *Proc. 8th Symposium of Thermophysical Properties* 298–302.

S. Horstmann; H. Gardeler; K. Fischer; F. Köster; J. Gmehling (2001): *Vapor Pressure, Vapor−Liquid Equilibrium, and Excess Enthalpy Data for Compounds and Binary Subsystems of the Chlorohydrin Process for Propylene Oxide Production*, J. Chem. Eng. Data **2**:337–345.

C.-C. Hu; P.-H. Chiu; S.-J. Wang; S.-H. Cheng (2015): *Isobaric Vapor–Liquid Equilibria for Binary Systems of Diethyl Carbonate + Propylene Carbonate, Diethyl Carbonate + Propylene Glycol, and Ethanol + Propylene Carbonate at 101.3 kPa*, J. Chem. Eng. Data **5**:1487–1494.

E. C. Ihmels; J. Gmehling (2001): *Densities of Toluene, Carbon Dioxide, Carbonyl Sulfide, and Hydrogen Sulfide Over a Wide Temperature and Pressure Range in the Sub- And Supercritical State*, Ind. Eng. Chem. Res. 4470–4477.

R. T. Jacobsen; R. B. Stewart (1973): *Thermodynamic Properties of Nitrogen Including Liquid and Vapor Phases from 63 K to 2000 K with Pressures to 10,000 Bar*, J. Phys. Chem. Ref. Data:757–922.

J. A. Jiménez; F. Martinez (2006): *Thermodynamic Study of the Solubility of Acetaminophen in Propylene Glycol + Water Cosolvent Mixtures*, J. Braz. Chem. Soc. **1**:125–134.

H. Kamerlingh Onnes (1901): *Expression of the Equation of State of Gases and Liquids by Means of Series*.

Y. Kayukawa; M. Hasumoto; K. Watanabe (2003): *Rapid Density Measurement System With Vibrating-Tube Densimeter*, Am. Inst. Phys.

A. F. Kazakov; C. D. Muzny; V. Diky; R. D. Chirico; M. Frenkel (2010): *Redictive Correlations Based on Large Experimental Datasets: Critical Constants for Pure Compounds*, Fluid Phase Equilib. 131–142.

I. S. Khattab; F. Bandarkar; M. Khoubnasabjafari; A. Jouyban (2013): *Density, Viscosity, Surface Tension, and Molar Volume of Propylene Glycol + Water Mixtures from 293 to 323 K and Correlations by the Jouyban-Acree Model*, Arab. J. Chem. 71–75.

T. Kishimoto; O. Nomoto (1954): *Absorption of Ultrasonic Waves in Organic Liquids (II) Liquids with Negative Temperature Coefficient of Sound Absorption (a) Glycols, Cyclohexanol and Cresol*, J. Phys. Soc. Jpn. **6**:1021–1029.

M. Köhler; P. Lunkenheimer; Y. Goncharov; R. Wehn; A. Loidl (2008): *Glassy Dynamics in Mono-, Di-, And Tri-Propylene Glycol: From the α- to the Fast β-Relaxation*, Cornell University Library 1–8.

T. S. Krishna; M. Gowri Sankar; K. R. Thomas; S. Govardhan Rao; B. Munibhadrayya (2015): *Acoustic, Volumetric, and Optic Study of Binary Mixture of 1-Butyl-3-Methylimidazoliumtetrafluoroborate With Propylene Glycols at T=(298.15 to 323.15) K*, J. Mol. Liq. 350–358.

K. K. Kundu; P. K. Chattopadhyay; D. Jana; M. N. Das (1970): *Standard Potentials of Ag-AgX (X=Cl or Br) Electrodes in Glycolic Solvents at Different Temperatures and Related Thermodynamic Quantities*, J. Chem. Eng. Data **2**:209–213.

S. K. Kushare; D. H. Dagade; K. J. Patil (2008): *Volumetric and Compressibility Properties of Liquid Water as a Solute in Glycolic, Propylene Carbonate, and Tetramethylurea Solutions at T=298.15 K*, J. Chem. Thermodyn. **1**:78–83.

S. V. Latha; G. Little Flower; K. Rayapa Reddy; C. V. Nageswara Rao; A. Ratnakar (2015): *Exploration of Volumetric, Acoustic, Thermodynamic and IR Studies of Binary Mixtures of Green Solvent Ethyl Lactate with C3 Alkanols at T=(303.15, 308.15, 313.15 and 318.15) K and Atmospheric Pressure*, J. Mol. Liq. 153–160.

H. Lee (1990): *Excess Molar Volumes of (Water + 1,2-Propanediol), (Methanol + 1,2-Propanediol), and (Water + Methanol + 1,2-Propanediol) at 283.15 K, 298.15 K, and 303.15 K*, J. Chem. Thermodyn. **5**:463–468.

E. W. Lemmon (2018): *Non-Linear Fitting Algorithm,* Private Communication to M. Thol.

E. W. Lemmon; I. H. Bell; M. L. Huber; M. O. McLinden (2018): *NIST Standard Reference Database 23: Reference Fluid Thermodynamic and Transport Propertie-REFPROP,* National Institute of Standards and Technology.

C.-K. Li; A. N. Soriano; M.-H. Li (2009): *Heat Capacities of the Mixed-Solvents Desiccants (Glycols+Water+Salts)*, Thermochim. Acta **1-2**:26–32.

Q.-S. Li; M.-G. Su; S. Wang (2007): *Densities and Excess Molar Volumes for Binary Glycerol + 1-Propanol, + 2-Propanol, + 1,2-Propanediol, and + 1,3-Propanediol Mixtures at Different Temperatures*, J. Chem. Eng. Data **3**:1141–1145.

Q.-S. Li; Y.-M. Tian; S. Wang (2008): *Densities and Excess Molar Volumes for Binary Mixtures of 1,4-Butanediol + 1,2-Propanediol, + 1,3-Propanediol, and + Ethane-1,2-diol from (293.15 to 328.15) K*, J. Chem. Eng. Data **1**:271–274.

J.-L. Ling; F. Cao; M. Xu; L. Yu (2011): *Density, refractive index and viscosity of binary mixture of ethyl acetate and 1,2-propanediol*, J. Chem. Ind. Eng. China **5**:1191–1196.

J.-L. Ling; L. Li; J.-L. Yang (2016): *Excess Molar Volumes and Viscosities of Binary Mixtures Composed of 1,2-Propanediol with Butanol, Pentanol or Hexanol*, J. Chem. Eng. Chinese Univ. **30(2)**:268–275.

D. M. Makarov; G. I. Egorov; A. M. Kolker (2016): *Temperature and Composition Dependences of Volumetric Properties of (Water + 1,2-Propanediol) Binary System*, J. Mol. Liq. 656–662.

M. K. Mamedov; A. G. Piraliev; R. A. Rasulova (2009): *Synthesis of Bicyclo [2.2.1] Heptyl Monoethers of Aliphatic Diols*, Russian Journal of Applied Chemistry **3**:518–520.

A. Marchetti; G. Pályi; L. Tassi; A. Ulrici; C. Zucchi (2000): *Variation of Volumic Properties with Temperature and Composition of 2-butanone + 1,2-Propanediol Binary Mixtures*, J. Mol. Liq. **2-3**:183–195.

Y. Marcus (1998): *The Properties of Solvents*, John Wiley & Sons 1–239.

G. W. Marks (1967): *Acoustic Velocity with Relation to Chemical Constitution in Alcohols*, J. Acoust. Soc. Am. **1**:103–117.

C. Marsden (1954): *Solvents and Allied Substances Manual - Propylene Glycol*, Cleaver-Hume Press LTD 322–323.

A. E. Martin; F. H. Murphy (2000): *Propylene Glycols*, DOW Chemical Company.

I. Martinez (1995): *Properties of Liquids,* Ciudad Univerisitaria. http://web-server.dmt.upm.es/~isidoro/.

T. Mathuni; J.-I. Kim; S.-J. Park (2011): *Phase Equilibrium and Physical Properties for the Purification of Propylene Carbonate (PC) and γ-Butyrolactone (GBL)*, J. Chem. Eng. Data **1**:89–96.

E. F. May; W. J. Tay; M. Nania; A. Aleji; S. Al-Ghafri; J. P. M. Trusler (2014): *Physical Apparatus Parameters And Model for Vibrating Tube Densimeters at Pressures to 140 MPa and Temperatures to 473 K*, Am. Inst. Phys.

P. J. Mohr; B. N. Taylor; D. B. Newell (2012): *CODATA Recommended Values of the Fundamental Physical Constants*, Rev. Mod. Phys. 1527-1603.

R. S. Musavirov; E. A. Kantor; D. L. Rakhmankulov (1978): *Reparation of Di-and Polyols by Transacentalization of 1,3 -Dioxacyloalkanes*, J. Appl. Chem. USSR **51**:2184–2187.

G. D. Nageshwar; P. S. Mene (1968): *Viscosity of the Ternary Liquid Mixture n-Butyl Acetate, Butanol-Propylene Glycol*, Indian Chem. Eng. 118–120.

A. K. Nain (2007): *Densities and Volumetric Properties of (Formamide+Ethanol, or 1-Propanol, or 1,2-Ethanediol, or 1,2-Propanediol) Mixtures at Temperatures Between 293.15K and 318.15K*, J. Chem. Thermodyn. **3**:462–473.

A. K. Nain (2008): *Ultrasonic and Viscometric Studies of Molecular Interactions in Binary Mixtures of Formamide with Ethanol, 1-Propanol, 1,2-Ethanediol and 1,2-Propanediol at Different Temperatures*, J. Mol. Liq. **1-3**:108–116.

M. Nicolae; F. Oprea (2014): *Vapor-Liquid Equilibrium for the Binary Mixtures of Dipropylene Glycol with Aromatic Hydrocarbons. Experimental and Regression*, Fluid Phase Equilib. 34–42.

J. D. Olson; D. C. Cordray (1992): *Thermodynamics of Hydrogen-Bonding Mixtures: GE, HE, and VE of Propylene Glycol + Ethylene Glycol*, Fluid Phase Equilib. **7**:213–223.

B. Orge; B. E. de Cominges; G. Marino; M. Iglesias; J. Tojo (2001): *Derived Properties of Binary Mixtures Containing (Acetone or Methanol) + Hydroxil Compounds*, Phys. Chem. Liq. **1**:99–116.

S. L. Outcalt; M. O. McLinden (2007): *Automated Densimeter For the Rapid Characterization of Industrial Fluids*, Ind. Eng. Chem. Res. 8264–8269.

A. Pal; M. Saini; B. Kumar (2016): *Volumetric, Ultrasonic and Spectroscopic (FT-IR) Studies for the Binary Mixtures of Imidazolium Based ILs with 1,2-Propanediol*, Fluid Phase Equilib. 66–73.

R. Palani; A. Geetha (2009): *Acoustical and Excess Thermodynamic Studies of Molecular Interaction in Aqueous Mixed Solvent Systems at 303, 308 and 313 K*, Phys. Chem. Liq. **5**:542–552.

G. S. Parks; H. M. Huffman (1927): *Studies on Glass. I The Transition between Glassy and Liquid States in the Case of Some Simple Organic Compounds*, J. Phys. Chem. **12**:1842–1855.

D. Peng; D. B. Robinson (1976): *A New Two-Constant Equation of State*, Ind. Eng. Chem. Res. **1**:59–64.

A. Pietrzak; K. Łudzik (2015): *Excess Volumes and Excess Heat Capacities of {1,2-Alkanediol+Methanol} Mixtures and Ionic Volumes in these Systems*, Fluid Phase Equilib. 56–63.

B. E. Poling *et al. (*2001): *The Properties of Gases and Liquids,* McGraw-Hill.

E. G. Ponedelnikova; V. V. Tarasova (1954): *The Generalization of Rao's Law for Associated Liquids*, Dok. Akad. Nauk SSSR 1191–1194.

T. T. Puck; H. Wise (1946): *Studies in Vapor–Liquid Equilibria. I. A New Dynamic Method for the Determination of Vapor Pressures of Liquids*, J. Phys. Chem. **4**:329–339.

N. V. Rane; A. Kumari; J. Soujanya; B. Satyavathi (2016): *Excess Properties and Isobaric (Vapor + Liquid) Equilibrium at Sub-Atmospheric Pressures of Binary (1,2-Propanediol + 1,3-Propanediol) System*, J. Chem. Thermodyn.142–157.

N. H. Rhys; R. J. Gillams; L. E. Collins; S. K. Callear; M. J. Lawrence; S. E. McLain (2016): *On the Structure of An Aqueous Propylene Glycol Solution*, J. Chem. Phys. 1–12.

J. A. Riddick; W. B. Bunger; T. K. Sakano (1986): *Techniques of Chemistry. 3. Physical Properties: Tabulations*, John Wiley & Sons.

J. A. Riddick; E. E. Toops, Jr. (1955): *Organic Solvents*, Techn. Org. Chem. 90–118.

C. M. Romero; M. S. Páez; D. Pérez (2008): *A Comparative Study of the Volumetric Properties of Dilute Aqueous Solutions of 1-Propanol, 1,2-Propanediol, 1,3-Propanediol, and 1,2,3-Propanetriol at Various Temperatures*, J. Chem. Thermodyn. **12**:1645–1653.

J. A. Ruddick (1971): *Toxicology, Metabolism, and Biochemistry of 1,2-Propanediol*, Toxicology and Applied Pharmacology 102–111.

A.Kh. Sadykov; D.I. Sagdeev; V.P. Brykov; G.Kh. Mukhamedzyanov (1974): *Density and Viscosity of Liquid Polyoxy Compounds*, Trudy Kazanskogo Khimiko-Tekhnologicheskogo Instituta 98–101.

D.I. Sagdeev; M.G. Fomina; I.M. Abdulagatov (2017): *Density and Viscosity of Propylene Glycol at High Temperautres and High Pressures*, Fluid Phase Equilib. 99–111.

M. A. Saleh; S. Begum; S. K. Begum; B. A. Begum (1999): *Viscosity of Dilute Aqueous Solutions of Some Diols*, Phys. Chem. Liq. **6**:785–801.

C. Sampson; X. Yang; Jue Xu; M. Richter (2018): *Measurement and Correlation of the (p, ρ, T) Behavior of Liquid Propylene Glycol at Temperatures from (272.7 to 393.0) K and Pressures up to 91.4 MPa*, to be submitted to Journal of Chemical Thermodynamics.

Y. A. Sanmamed; D. Gonzalez-Salgado; J. Troncoso; C. A. Cerdeirina; L. Romaní (2007): *Viscosity-Induced Errors in the Density Determination of Room Temperature Ionic Liquids Using Vibrating Tube Densitometry*, Fluid Phase Equilib. 96–102.

N. V. Sastry; M. C. Patel (2003): *Densities, Excess Molar Volumes, Viscosities, Speeds of Sound, Excess Isentropic Compressibilities, and Relative Permittivities for Alkyl (Methyl, Ethyl, Butyl, and Isoamyl) Acetates + Glycols at Different Temperatures*, J. Chem. Eng. Data **4**:1019–1027.

O. J. Schierholtz; M. L. Staples (1935): *Vapor Pressures of Certain Glycols*, J. Am. Chem. Soc. **12**:2709–2711.

C. Scholz (2017): *Speed of Sound Measurements for Pentane, Hexane, Heptane, and Propylene Glycol,* Private Communication to M. Thol.

U. Setzmann; W. Wagner (1991): *A New Equation of State and Tables of Thermodynamic Properties for Methane Covering the Range from the Melting Line to 625 K at Pressures up to 100 MPa*, J. Phys. Chem. Ref. Data 1061–1155.

L. M. Sevgili; S. Şahin; Ş. I. Kırbaşlar (2008): *Liquid−Liquid Equilibria of (Limonene + Linalool + Ethylene Glycol or Diethylene Glycol or Triethylene Glycol or 1,2-Propylene Glycol) Ternary Systems*, J. Chem. Eng. Data **3**:737–741.

Y. Shi; W. Li; J. Tu (1999): *Methanol-Isoamyl Acetate, Dimethyl Carbonate-Isoamyl Acetate and Methanol-1,2-Propanediol - Liquid-Vapour Equilibrium Data of Measurement and Correlation*, Gaoxiao-huaxue-gongcheng-xuebao **2**:147–151.

G. Soave (1980): *Rigorous and Simplified procedures for Determining the Pur-Component Parameters in the Redlich-Kwong-Soave Equation of State*, Chem. Eng. Sci. **8**:1725–1730.

N. M. Sokolov; L. N. Tsygankova; M. I. Shtrom; N. M. Zhavoronkov (1972): *Seperation of a 1,2-Propylenglycol - Ethylenglycol Mixture at Different Pressures*, Sov. Chem. Ind. **7**:427–429.

N. M. Sokolov; L. N. Tsygankova; N. M. Zhavoronkov (1971): *The Liquid - Vapor Equilibrium in the Water - Ethylene Glycol and Water - 1,2 - Proylene Glycol Systems at Various Pressures*, Theor. Found. Chem. Eng. **6**:817–820.

D. A. Soldatović; J. M. Vuksanović; I. R. Radović; M. L. Kijevčanin (2016): *Thermodynamic and Spectroscopic Interpretation of Molecular Interactions of Nicotine + Alcohol Binary Mixtures*, J. Chem. Thermodyn. 105–129.

R. Span (2000): *Multiparameter equations of state: An accurate source of thermodynamic property data,* Sprinter-Verlag.

D. R. Stull (1947): *Vapor Pressure of Pure Substances - Organic Compounds*, Indian Chem. Eng. **4**:517–540.

D. Subramanian; G. D. Nageshwar; P. S. Mene (1978): *Isobaric Vapour Liquid Equilibrium Data for N-Amyl Alcohol and Iso-Amyl Alcohol with Propylene Glycol*, Petrol. Chem. Ind. Dev. 9–11.

T. Sun; A. S. Teja (2004): *Density, Viscosity and Thermal Conductivity of Aqueous Solutions of Propylene Glycol, Dipropylene Glycol, and Tripropylene Glycol between 290 K and 460 K*, J. Chem. Eng. Data **5**:1311–1317.

M. Thol (2015): *Empirical Multiparameter Equations of State Based on Molecular Simulation and Hybrid Data Sets,* Ruhr-Universität Bochum.

M. Thol; G. Rutkai; R. Span; J. Vrabec; R. Lustig (2015): *Equation of State for the Lennard-Jones Truncated and Shifted Model Fluid*, Int. J. Therm. 25–43.

M. J. Timmermans; Hennaut-Roland (1955): *Travaux du bureau international d'étalons physico-chimiques*, J. Chim. Phys. 223–245.

K. Trachenko; V. V. Brazhkin (2011): *Heat Capacity at the Glass Transition*, Physical Review B 1–6.

C.-Y. Tsai; A. N. Soriano; M.-H. Li (2009): *Vapour Pressures, Densities, and Viscosities of The Aqueous Solutions Containing (Triethylene Glycol or Propylene Glycol) and (LiCl or LiBr)*, J. Chem. Thermodyn. **5**:623–631.

N. G. Tsierkezos; M. M. Palaiologou (2009): *Ultrasonic Studies of Liquid Mixtures of Either Water or Dimethylsulfoxide With Ethylene Glycol, Diethylene Glycol, Triethylene Glycol, Tetraethylene Glycol, 1,2-Propylene Glycol and 1,4-Butylene Glycol at 298.15 K*, Phys. Chem. Liq. **4**:447–459.

VDI Wärmeatlas (2013): *Berechnung der spezifische isobare Wärmekapazität idealer Gase mit der Gruppenbeitragsmethode nach Joback*, VDI e.V. VDI-Gesellschaft Verfahrenstechnik und Chemieingenieurwesen 156–158.

G. Venkatarathnam; L. R. Oellrich (2011): *Identification of the Phase of a Fluid Using Partial Derivatives of Pressure, Volume, and Temperature Without Reference to Saturation Properties: Applications in Phase Equilibria Calculations*, Fluid Phase Equilib. 225–233.

S. P. Verevkin (2004): *Determination of Vapor Pressures and Enthalpies of Vaporization of 1,2-Alkanediols*, Fluid Phase Equilib. **1**:23–29.

S. P. Verevkin; V. N. Emel'yanenko; G. Nell (2009): *1,2-Propanediol. Comprehensive Experimental and Theoretical Study*, J. Chem. Thermodyn. **10**:1125–1131.

A.N. Vinogradov; M.I. Shakhparonov (1984): *Acoustical properties of 1,2-propanediol and its solutions in water and propanol*, Viniti Code 1–27.

D. M. VonNiederhausern; G. M. Wilson; N. F. Giles (2000a): *Critical Point and Vapor Pressure Measurements at High Temperatures by Means of a New Apparatus with Ultralow Residence Times*, J. Chem. Eng. Data 157–160.

D. M. VonNiederhausern; L. C. Wilson; N. F. Giles; G. M. Wilson (2000b): *Critical-Point Measurements for Nine Compounds by a Flow Method*, J. Chem. Eng. Data **2**:154–156.

W. Wagner; A. Pruss (2002): *The IAPWS Formulation 1995 for the Thermodynamic Properties of Ordinary Water Substance for General and Scientific Use*, J. Phys. Chem. Ref. Data **2**:387–535.

W. Wagner; R. Span (1993): *Special Equations of State for Methane, Argon, and Nitrogen for the Temperature Range from 270 to 350 K at Pressures up to 30 MPa*, Int. J. Therm. **4**:699–725.

M. E. Wieser; M. Berglund (2009): *Atomic Weights of the Elements 2007 (IUPAC Technical Report)*, Pure Appl. Chem. **11**:2131–2156.

W. V. Wilding; L. C. Wilson; G. M. Wilson (1991): *Vapor-Liquid Equilibrium Measurements on Eight Binary Mixtures: DIPPR Projects 805(A)/89 and 805(E)/89*, AlChE Data Series 6–23.

L. C. Wilson; W. V. Wilding; G. M. Wilson (1989): *Vapour-Liquid Equilibrium Measurements on Four Binary Mixtures*, AlChE Symp. Ser. **271**:25–43.

L. C. Wilson; W. V. Wilding; H. L. Wilson; G. M. Wilson (1995): *Critical Point Measurements by a New Flow Method and a Traditional Static Method*, Am. Chem. Soc. 765–768.

R. Xie; C. Chen (1993): *Experimental Research on Method of Vapor-Pressure Measurement*, J. Chem. Eng. Chinese Univ. **7**:267–271.

C. Yang; X. Feng; Y. Sun; Q. Yang; J. Zhi (2015): *Isobaric Vapor–Liquid Equilibrium for Two Binary Systems{Propane-1,2-diol + Ethane-1,2-diol and Propane-1,2-diol + Butane-1,2-diol} at p = (10.0, 20.0, and 40.0) kPa*, J. Chem. Eng. Data **4**:1126–1133.

A. Zander (1882): *Über die spezifischen Volumina Einiger Allyl-Propyl-und Verwandter Verbindungen*, Justus Liebigs Ann. Chem. **214**:138–193.

H. Zarei; S. A. Golroudbari; M. Behroozi (2013): *Experimental Studies on Volumetric and Viscometric Properties of Binary and Ternary Mixtures of N,N-Dimethylacetamide, N-Methylformamide and Propane-1,2-Diol at Different Temperatures*, J. Mol. Liq. 260–265.

H. A. Zarei; S. Asadi; H. Iloukhani (2008): *Temperature Dependence of the Volumetric Properties of Binary mixtures of (1-Propanol, 2-Propanol and 1,2-Propanediol) at Ambient Pressure (81.5 kPa)*, J. Mol. Liq. **1-2**:25–30.

H. A. Zarei; N. Mirhidari; Z. Zangeneh (2009): *Densities, Excess Molar Volumes, Viscosity, and Refractive Indices of Binary and Ternary Liquid Mixtures of Methanol (1) + Ethanol (2) + 1,2-Propanediol (3) at P = 81.5 kPa*, J. Chem. Eng. Data **3**:847–854.

K. Zemánková; J. Troncoso; L. Romaní (2013): *Excess Volumes and Excess Heat Capacities for Alkanediol+Water Systems in the Temperature Interval (283.15–313.15)K*, Fluid Phase Equilib. 1–10.

L. Zhang; W. Wu; Y. Sun; L. Li; B. Jiang; X. Li; N. Yang; H. Ding (2013): *Isobaric Vapor–Liquid Equilibria for the Binary Mixtures Composed of Ethylene Glycol, 1,2-Propylene Glycol, 1,2-Butanediol, and 1,3-Butanediol at 10.00 kPa*, J. Chem. Eng. Data **5**:1308–1315.

Y. Zhong; Y. Wu; J. Zhu; K. Chen; B. Wu; L. Ji (2014): *Thermodynamics in Separation for the Ternary System 1,2-Ethanediol + 1,2-Propanediol + 2,3-Butanediol*, Ind. Eng. Chem. Res. **30**:12143–12148.

Zhou; E. W. Lemmon (2018): *Equation of State for Ethylene Glycol,* Private Communication to M. Thol.

V. I. Zhuravlev (1992): *Structure of Multiatomic Alcohols and Their Solutions According to the Dielectric-Spectroscopy Data - Equilibrium and Dynamic Properties of Propanediols*, Zh. Fiz. Khim. 225–236.

V. I. Zhuravlev; V. A. Durov; T. M. Usacheva; M. I. Shakhparonov (1985): *Dielectric Spectroscopy of 1,2-Propanediol-1-Propanol Solutions*, Zh. Obshch. Khim. **55(5)**:992–996.

E. M. Zivković; D. M. Bajić; I. R. Radović; S. P. Šerbanović; M. L. Kijevčanin (2014): *Volumetric and Viscometric Behavior of the Binary Systems Ethyl Lactate+1,2-Propanediol, +1,3-Propanediol, +Tetrahydrofuran and +tetraethylene glycol dimethyl ether. New UNIFAC–VISCO and ASOG–VISCO parameters determination*, Fluid Phase Equilib. 1–19.

J. A. Zollweg; G. W. Mulholland (1972): *On the Law of the Rectilinear Diameter*, J. Chem. Phys. **3**:1021–1025.

E. Zorebski; M. Dzida; M. Piotrowska (2008): *Study of the Acoustic and Thermodynamic Properties of 1,2- and 1,3-Propanediol by Means of High-Pressure Speed of Sound Measurements at Temperatures from (293 to 318) K and Pressures up to 101 MPa*, J. Chem. Eng. Data **1**:136–144.

E. Zorebski; A. Przybyła (2013): *Volume Effects for Binary Mixtures of Propane-1,2-diol with Methanol, Propan-1-ol, Hexan-1-ol, Octan-1-ol, or Nonan-1-ol at Temperatures (293.15 to 318.15)K*, J. Chem. Thermodyn. 127–134.